



LUND UNIVERSITY

Unconventional Magnetic Actuators for Automatic Transmission Shifted by Wire

Reinap, Avo

2015

[Link to publication](#)

Citation for published version (APA):

Reinap, A. (2015). *Unconventional Magnetic Actuators for Automatic Transmission Shifted by Wire*. [Publisher information missing].

Total number of authors:

1

General rights

Unless other specific re-use rights are stated the following general rights apply:

Copyright and moral rights for the publications made accessible in the public portal are retained by the authors and/or other copyright owners and it is a condition of accessing publications that users recognise and abide by the legal requirements associated with these rights.

- Users may download and print one copy of any publication from the public portal for the purpose of private study or research.
- You may not further distribute the material or use it for any profit-making activity or commercial gain
- You may freely distribute the URL identifying the publication in the public portal

Read more about Creative commons licenses: <https://creativecommons.org/licenses/>

Take down policy

If you believe that this document breaches copyright please contact us providing details, and we will remove access to the work immediately and investigate your claim.

LUND UNIVERSITY

PO Box 117
221 00 Lund
+46 46-222 00 00

Unconventional Magnetic Actuators

Automatic Transmission Shifted by Wire



Avo Reinap

Division of Industrial Electrical Engineering and Automation
Faculty of Engineering, Lund University

Summary

This is a technical report that collects the highlights on the development of an unconventional magnetic actuator (UMA) for Automatic Transmission Shifted by Wire (ATSbW). This work is carried out with the support of FFI Vinnova and this support is gratefully acknowledged.

Shortly, ATsbW application requires a compact and inexpensive electrically actuated drive that provides high torque over limited angle of movement. The specific research focus of this project is related to a development and analysis of a novel and unconventional solutions for transmission actuators. The central part of the subsystem is electromagnetic actuator that either directly performs the system requirements or is integrated into mechanical transmission that completes the task. The following transmission actuators are examined in this report:

1. Direct electromagnetic actuators based on **magnetic memory materials** and magnetic interaction of **magnetic shear forces** like in a conventional rotating machines
2. Integration of an electromagnetic actuator into a **harmonic gear** by taking advantage of **compression and repulsion forces**
3. Integration of an electromagnetic actuator into a **cycloid gear** by taking advantage of **compression forces**

Writing this report is inspired by technical discussions and negotiations during the course of this project from early 2013 to summer 2015. Sincere gratitude is hereby expressed to all those who contributed to this work among them Björn Carlberg, Bengt Cyren, Tomas Wykman, Jasmin Insanic, Claes Rundqvist, Henrik Nilsson, Mats Alaküla, Getachew Darge, Jan Folkhammar, Lennart Edström, Åke Nyström, Thomas Rundqvist, Tord Cedell and some others who has not been listed above.

Content

Summary.....	1
Content.....	2
1 System requirements and architecture.....	3
1.1 Classification of topologies	3
1.2 System architecture and integration.....	4
2 Direct actuators.....	7
2.1 Actuation based on volumetric forces of magnetic memory materials.....	7
2.2 Actuation based on surface shear forces between the bodies	8
3 Actuator integrated into a harmonic drive.....	9
3.1 Electrically driven wave generator	9
3.2 Magnetically deformed wave generator.....	11
4 A cycloid gear integrated into an electrical machine	16
4.1 Electromagnetic clogged cycloid.....	16
4.2 Electromagnetic friction cycloid.....	22
4.3 Control and selection of power electronic controller	41
5 Conclusions.....	42
References	43

1 System requirements and architecture

By starting the rough geometric layout, ca 1dm³ volume of the tight sealed system should deliver 20Nm peak over the limited angular motion on the output hollow or a shaft. The list of design prerequisites are

1. Size constrains ca 10x10x10 cm → ca 1dm³ (IP66K..IP6K9K)
2. Limited angular motion 1/8 of revolution (48°)
3. Max shift torque 20 Nm (this requires more than 10-20 Nm/kg)
4. Actuation time P-R 150 ms, P-D 250 ms → ca ¼ rps = 15 rpm → ca 50 W/kg
 - a. Nominal shift torque 200,000 cycles P-D-P
 - b. Max shift torque 2000 8s cycles P-R-P
5. Temperature range $\vartheta_{amb} = -40..+130$ deg C,
6. Supply voltage range $U_{sup} = 9..16$ max 24 V

The imaginable layout for the system realization can be a hollow cylinder with one end closed and another open with the mechanical interface for the torque transmission. In order to provide possible solutions for system integration and assembly a number of different electromagnetic actuators are studied from

- direct torque capability point of view and
- applied magnetic forces point of view: tangential or normal comparing to the magnetized surfaces of the moving body

1.1 Classification of topologies

The central part of the transmission actuator topology is the **electromechanical energy converter**: conventional rotating machine or an unconventional magnetic actuator. The electromechanical energy conversion takes place at the presence of magnetism and the force mechanism can be seen as the forces between surfaces e.g. magnets or volumetric forces due to magnetic domain orientation in the magnetic materials. In this group are magnetostrictive and magnetic memory materials. The force action due to magnetic surfaces is divided between magnetic and reluctance origin depending whether two magnets counteract or one magnet attracts ferrous details in vicinity. Figure 1.1 shows the classification tree of magnetic actuators for ATsbW application. This chart (Figure 1.1) is incomplete as it does not show different electrical machine topologies under multi-pole block.

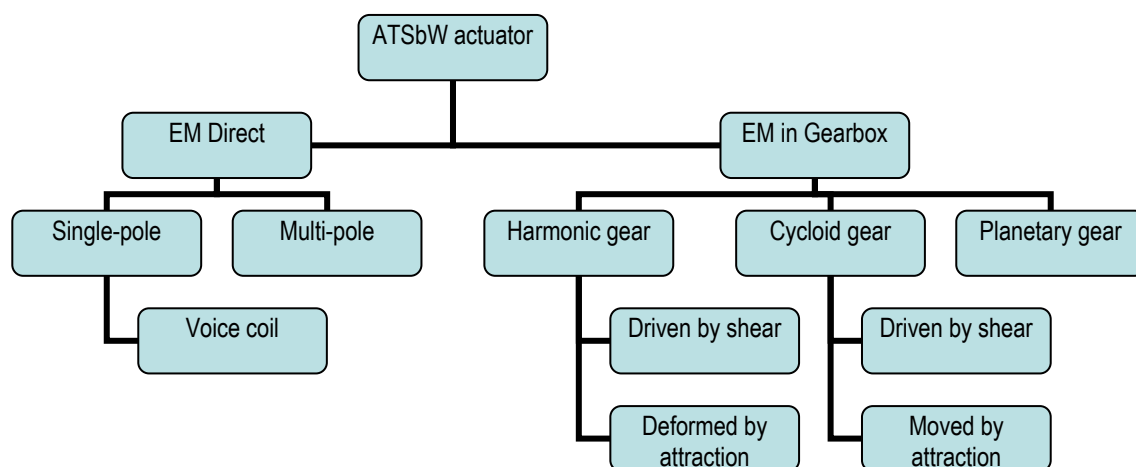


Figure 1.1 Transmission actuator topology mapping

This branch that illustrates the integration of electromagnetic actuators to different gearboxes concentrates the focus on harmonic and cycloid gear and excludes all other mechanical transmissions. There are a number of **general judgments** relating to selection of transmission actuators and these are listed below:

- Direct drive is rather bulky and unattractive due to fact that force and torque is directly proportional to the size. Therefore requirement for high force and torque can lead to unnecessary high weight and volume
- Geared drive or gearbox-on-gearbox becomes more attractive due to size reduction. This turns the focus more to mechanical engineering and assembling rather than exploration on alternative actuator concepts
- Harmonic drive is compact and has high gear ratio. There are already existing electric drives with harmonic drive speed reduction. A hasty conclusion, a new unconventional type of direct magnetic actuation by direct magnetic deformation seems challenging [6]
- Cycloid gear is another mechanical transmission that allows considerable speed and size reduction and is comparable to harmonic drives. The replacement of eccentric rotational input can be replaced by direct electromagnetic actuation of a cycloid disc

Summary, the direct electromagnetic actuator seems possible but not suitable for ATSBW application. This type of actuator is studied for comparison purposes. The main focus is kept on unconventional actuators rather than on a mechanic design of a suitable mechanic transmission for a conventional electrical motor that suite to ATSBW application. Therefore the integration of electromagnetically actuated harmonic or cycloid gear becomes some of the challenging targets.

1.2 System architecture and integration

Obviously there is a **tradeoff** between the input from electrical and mechanical engineering when it comes to the integration of the complete actuator. In this matter the complete system is divided into two parts as the blocks for the system architecture. The third subject is related how the blocks are united into a complete system:

1. Electromagnetic actuator
2. Mechanic transmission
3. Depth of integration

In order to solve the system architecture the **torque size relation** of the components are needed. A number of finite element (FE) models of a surface mounted permanent magnet synchronous machine (PMSM) is modeled with a following model input

- Outer radius of the electrical machine: $R_o=20\dots60$ mm
- Number of poles: $N_p=6\dots10$
- Peak value of current density in the winding: $J_c=5, 10, 15, 20$ A/mm²
- Volumetric size difference between rotor and stator: $K_z=1/\sqrt{2}, 1/\sqrt{3}, 1/\sqrt{4}$

The volumetric size difference is defined as air-gap radius R_g ratio to outer radius R_o of the machine:

$$K_z = \frac{R_g}{R_o} = \sqrt{\frac{\pi R_g^2 L}{\pi R_o^2 L}} = \sqrt{\frac{\pi R_g^2 L}{\pi (R_o^2 - R_g^2) L + \pi R_g^2 L}} = \sqrt{\frac{V_{rt}}{V_{st} + V_{rt}}} = \frac{1}{\sqrt{1 + \frac{V_{st}}{V_{rt}}}} \quad 1.1$$

This radius difference is related to rotor and stator volumes, respectively V_{rt} and V_{st} . The volumetric size difference is defined as $V_{st}=1V_{rt}$, $V_{st}=2V_{rt}$ and $V_{st}=3V_{rt}$.

The graphical layout of the PMSM including the flux density distribution is shown in Figure 1.2. The thickness of the permanent magnets and the air-gap is changed as a function of outer radius. Most of the other design parameters have the same proportional relation in respect to size of the machine. Initially the active (stator core stacking) length is taken equal to the outer diameter of the stator core.

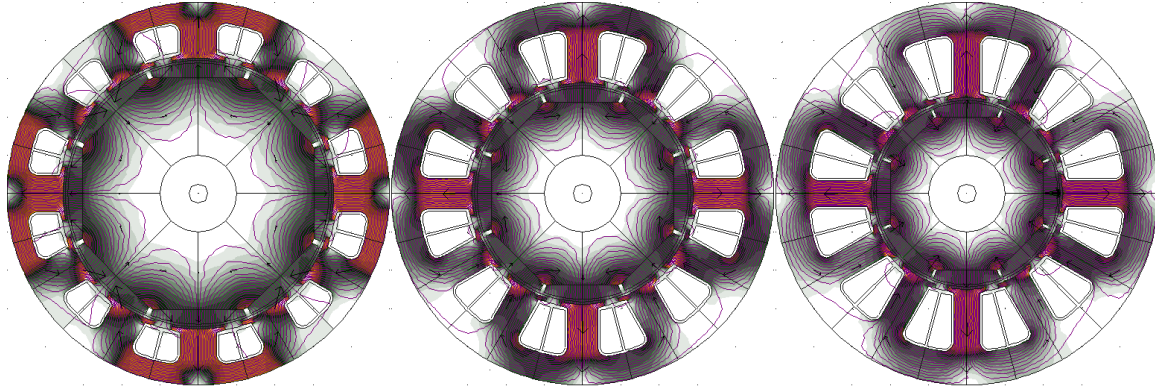


Figure 1.2 Models for electrical machines defining the magnetic shear stress, where left $V_{st}=V_r$, middle $V_{st}=2V_r$ and right $V_{st}=3V_r$ defines the machine layout.

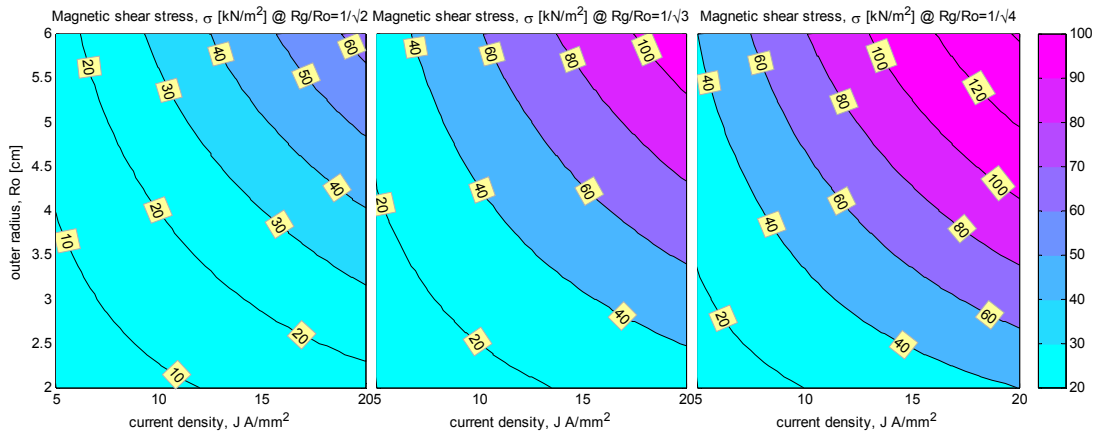


Figure 1.3 Magnetic shear stress as a function of current density outer radius of the stator core

As an outcome from the FE modeling of PMSM the magnetic shear stress (Figure 1.3) is calculated as a function of machine outer radius, volumetric size ratio of rotor to stator and the current density in the windings. Without going into deeper thermal analysis 10A/mm² is selected as a reference current density for selection of the **realistic magnetic shear stress** for PMSM.

Similar to produced shear stress for electrical machines that couples the electromagnetics to mechanics the gears have similar **gear transmission stress** – K-factor that is used to dimension the gears in respect of materials and load cycles related to applications [9][16]. This is basically the mechanical contact load stress that the flank of the working tooth surface has to maintain. The specific transmission volume is related to gear ratio, durability defined by K-factor and the specified torque. Usually this is defined from high speed driven pinion gear point of view:

$$d_1^2 b = \frac{2T_1}{K} \left(\frac{m_g + 1}{m_g} \right) \quad m_g = \frac{N_2}{N_1} = \text{gear ratio} \quad 1.2$$

From system architecture point of view it is important to gauge the transmission type and the achievable reduction rate for the transmissions. First an approximate weight of offset and planetary gears is estimated. The weight of the active volume for the mechanical transmission is calculated from a sizing equation and at the selected K factor of 1000kN/m² [9][16]. This estimation does not include the housing and supporting structures. Another approach is used for a harmonic gear. In this case a standard product series (HFUC) from Harmonic Drive AG is selected to define weight of the gear unit that is able to deliver at least 20 Nm at rated condition. Usually the larger units can provide gear ratio from 30 to 160 that smaller units are can not. Therefore two different gear sizes (17 and 20) are selected to provide the wide range for gear ratio of interest. The range of gear ratio (Figure 1.4) is defined as

- Basic range for gear ratio is from 1:1 to 1:10 by step of one and shown from cyan to magenta in Figure 1.4. First group in this figure shows the active weight needed for electrical machine (uncolored bars) and single stage offset gear (colored bars). Obviously 1:1 gear is not used and all 20 Nm output torque need to be provided directly by electrical machine.
- The second group of color bars in Figure 1.4 shows the estimated weight for the double stage offset gears and the corresponding electrical machine weight that all together is able to produce 20 Nm on output axel. The resulting range for gear ratio is from 1:1, 1:4 to 1:100.
- The third group demonstrates the expected active weight for integration where planetary gear is used for mechanical transmission. In this case the visible range for gear ratio is from 1:3 to 1:10.
- Two last groups of color bars demonstrate the expected integration of harmonic drive with electrical machine. The selected gear ratio is from 1:20 to 1:200 by step of 20. The size for harmonic transmission is selected according to rated output torque >20Nm and gear ratio. Complete gear unit (HFUC-2UH) is compared to a component set (HFUC-2A).

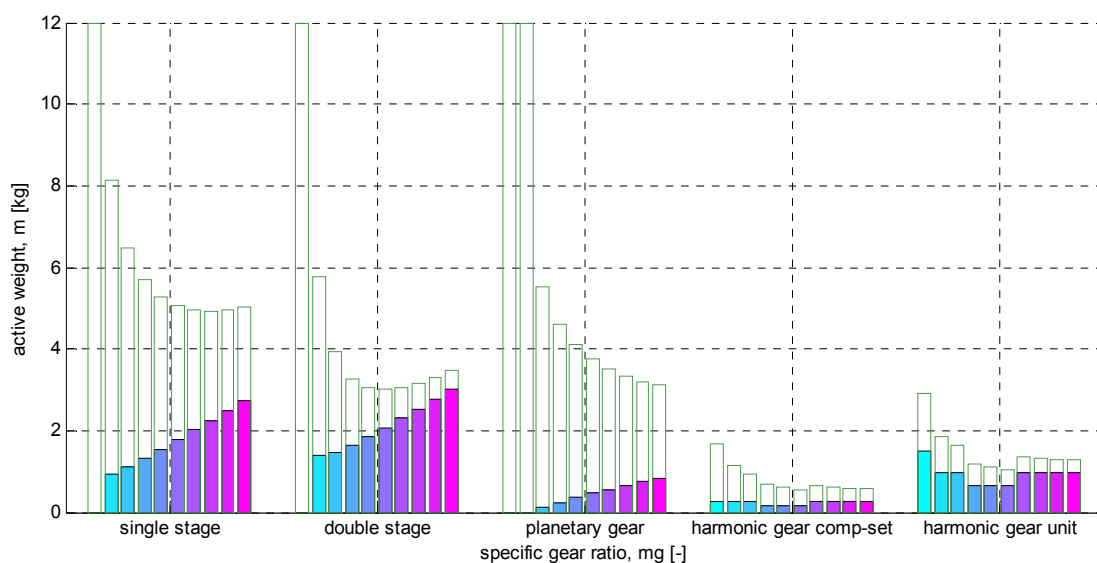


Figure 1.4 Weight estimation of active components in the system that can provide 20Nm on the output axel. Low gear is shown in cyan and high gear in magenta.

Summary, The functionality integration and the torque split between electromechanical actuator and reduction gears demonstrate the way towards mechanical transmission with high gear ratio. High gear ratio reduces the torque that electrical machine need to produce therefore the machine becomes smaller even if it does not provide as high magnetic stress than large machines. It is believed that cycloid gear can provide nearly the same gear reduction than harmonic drive and become attractive solution that provides higher efficiency [11].

2 Direct actuators

There are two appealing reasons for looking direct electromagnetic actuators

1. Magnetic anisotropic materials that provide large forces and strain under the influence of the applied magnetic field
2. High magnetic shear stresses between the magnets that can fulfill the application requirements for torque

2.1 Actuation based on volumetric forces of magnetic memory materials

Broadly the materials that change their shape under the influence of the magnetic field due to material anisotropy are magnetic shape memory alloys and magnetostrictive materials (Table 2.1). Magnetostrictive materials grow along the field direction and magnetic memory materials grow in transverse of the field direction. Magnetic memory materials grow considerably longer than magnetostrictive materials for a given field. It is easier to arrange the magnetization as the excitation coils can be beside the magnetic memory material and not around like it is typically solved for magnetostrictive materials.

Table 2.1 Magnetic strain materials

Magnetic material	Type	Strain	Magnetic field	Temperature
Terfenol-D	Magnetostriction	0.2%	160 kA/m	room
AdaptaMat	Memory alloy	9%		room

Initially, the starting point for the magnetic shape memory (MSM) actuator is based on three distributed single axis actuators that all together operate as a conventional three phase system that causes translatory movement on xy-plane. This motion is used to force the outer ring to rotate similarly to the action in the cycloid gear (Figure 2.1).

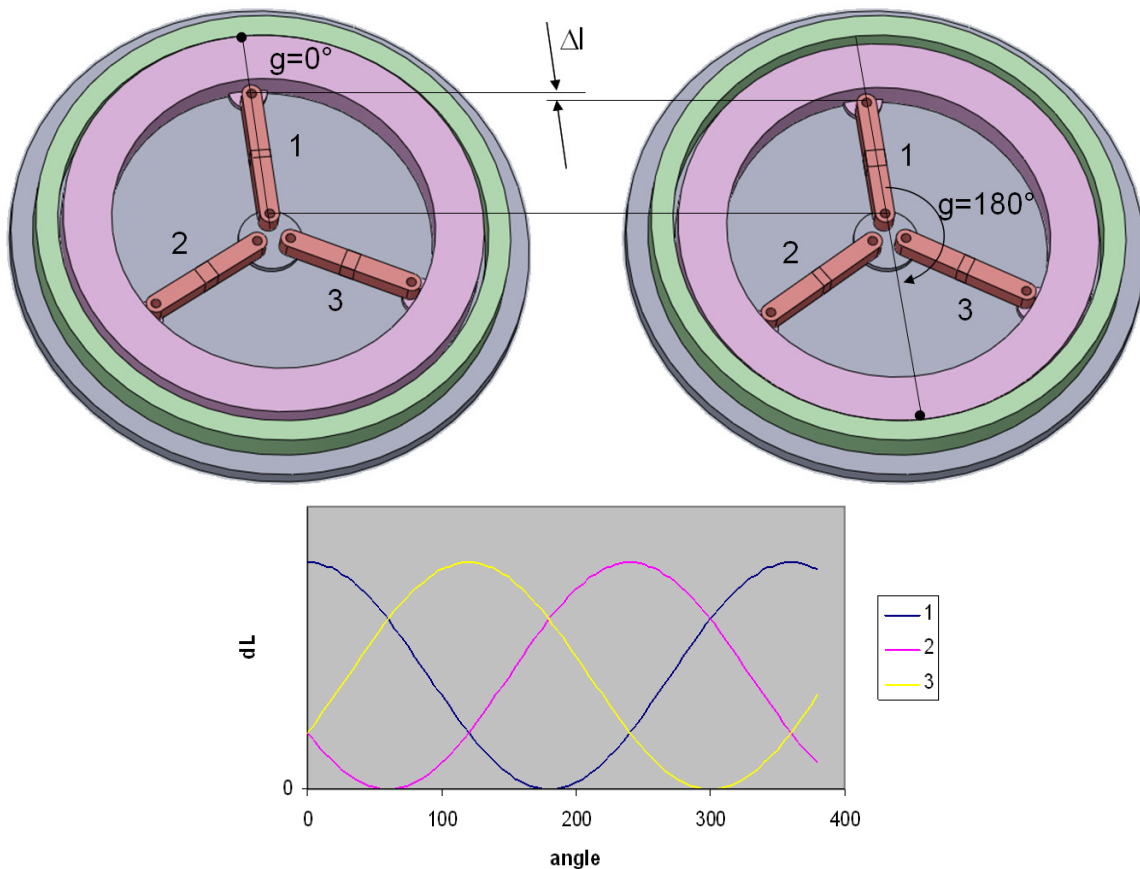


Figure 2.1 Initial concept for the actuator (above) and a relative elongation of the MSM rods as an outcome of control

Summary: the deeper study for the material properties and the design of suitable magnetizer has shown that the magnetizer becomes too large and the performance does not meet the specification requirements due to change of magnetic properties as a function of elongation and high temperature dependence of the material.

2.2 Actuation based on surface shear forces between the bodies

The high value of magnetic shear stress (above 100 kN/m² for medium size electrical machines) is inspiring the idea of a direct gear free transmission. Apart from a single phase solution, so called voice coil actuator a trial for a three phase sector machine is given. The geometric dimensions for the sector machine are following:

- Outer radius $R_o=80\text{mm}$, rotor turns out from bounding box
- Active or stacking height 60 mm, additional axial space required for the end-turns and housing
- 3.5 mm thick NdFe surface mounted magnets

The maximum current supposes to be defined as a result from the consequence of the heat pulse vs the available relaxation time. Alternatively a maximum current density of 10 A/mm² is defined for a compact coils that are premade from round wire and have a fill factor of 80 %. The current input is selected to reach the desired outcome of 20 Nm. The other results from this study is shown in Figure 2.2 and listed below:

- Shear stress 43.8 kN/m²
- Hot spot 264 °C at continuous operation with coil conductivity of 0.5 W/mK and scaled convection of 200 W/m²K at inner radius of the stator.

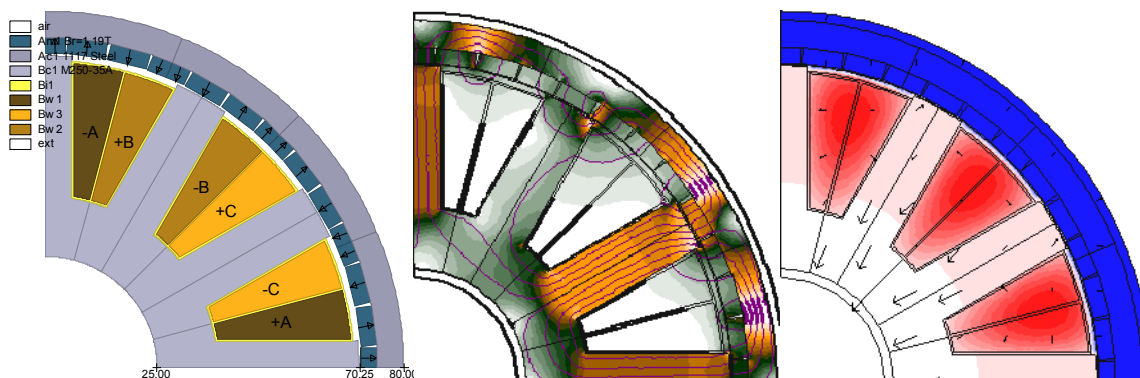


Figure 2.2 Direct driven or gearless transmission actuator: (left) layout of the actuator with surface mounted magnets and 3-phase concentrated windings, (middle) flux density distribution at loaded condition, and (right) temperature distribution at electrically loaded and thermally continuous operation point

Summary, this study shows that direct electromagnetic actuator is fully possible to provide the desired peak torque without becoming huge and bulky. At the same time this solution is far to be cost optimal for the application. There are also the other solutions that bases on the same idea of direct electromagnetic actuation, which are a toroidal and multi-pole configurations, but these are not presented here.

3 Actuator integrated into a harmonic drive

Compact, lightweight and high gear–ratio, these are some of the attractive features of harmonic drive or strain wave gearing. Similarly, the attractive features for electrical machine, which are compactness and lightweight, are more feasible at higher rotation speed when the torque and weight can be reduced for the same power. Therefore the integration of harmonic drive unit into electromagnetic actuator is an interesting option for ATSbW application. Conceptually, there are more options than two, but both of the methods are based on the arrangement of the wave generator.

- Option 1 is **electrically driven** elliptical disk with an outer ball bearing or a less complex roller arrangement in one axis that causes the gearing contact. The electrical machine is parallel to harmonic drive in assembling point of view and this is a task of merging standard components and this is already used in practice.
- Option 2 is based on **electromagnetic deformation** that aim is to integrate electrical machine into strain gearing action where the innermost part of the wave generator is replaced with an electromagnet that modulates the flex spline. The modulation in this case means the creation of mechanic gearing connection points due to magnetic compressive and repulsive forces.

Figure 3.1 indicates the specific parts of the harmonic drive.

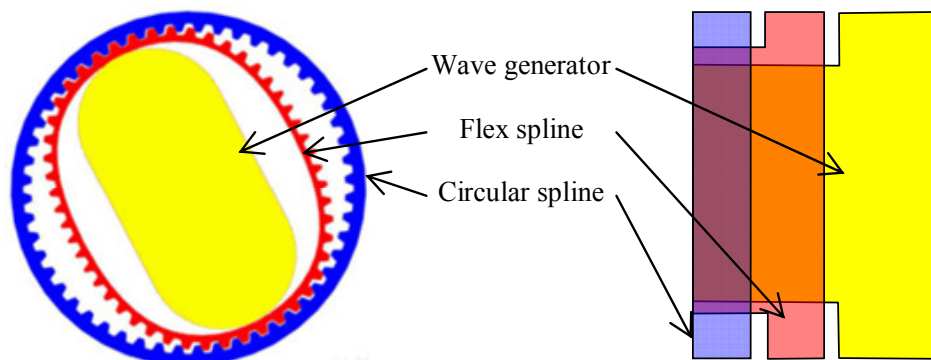


Figure 3.1 Principal sketch of harmonic drive: Outer circular spline (CS), inner wave generator (WG) and intermediate flex spline (FS)

$$ratio = \frac{N_{FlexSpline} - N_{CircularSpline}}{N_{FlexSpline}} = \frac{-2}{N_{FlexSpline}} \quad 3.1$$

3.1 Electrically driven wave generator

This concept bases on an integration of standard components: a rotating electrical machine and a harmonic gear into a single system. There are a number of existing solutions for the parallel integration by Harmonic Drive AG (www.harmonicdrive.de). The challenges seen from this project point of view are the cost drivers for a simpler system with reasonable gear ratio and efficiency. The replacement of an expensive elliptic bearing and using plastic materials for flex spline attracts interest while the moderate efficiency and the maximal output load for a given size constrain the attention.

A harmonic drive gear unit size 17 provides output torque around 20Nm: HFUC-17-xx-2A-R is selected from the product list of Harmonic Drive AG for a further integration study. Table 3.1 shows the main parts of a harmonic gear unit. In this integration study an outer rotor motor with a sliding roller contact is replacing the inner shaft and the wave generator with elliptic bearing. The rolling contact between the outer rotor and flex spline causes the revolving deformation and speed reduction from high speed input to low speed output.

Table 3.1 shows the component reduction of the conventional gear unit and Figure 3.2 shows the proposed integration of an electrical machine into the exiting parts harmonic gear.

Table 3.1 Component reduction from the conventional gear unit in order to integrate the electrical machine into it

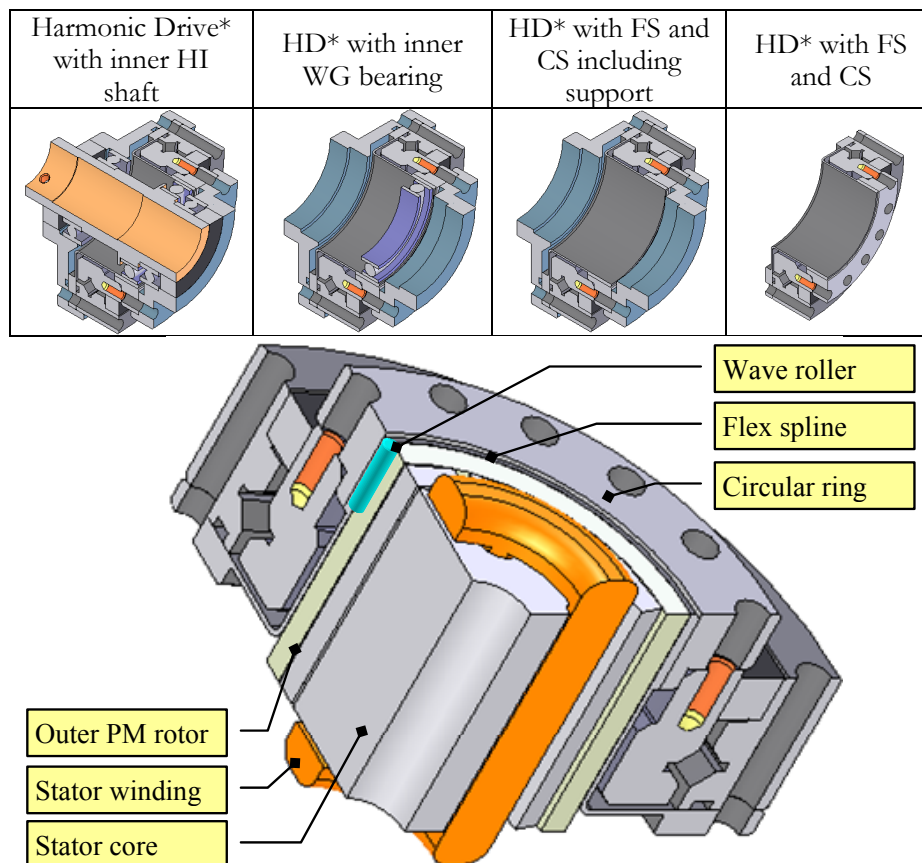


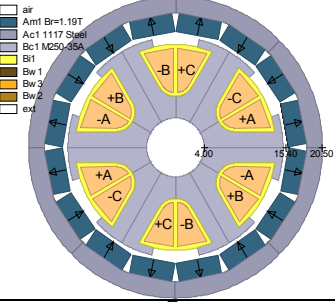
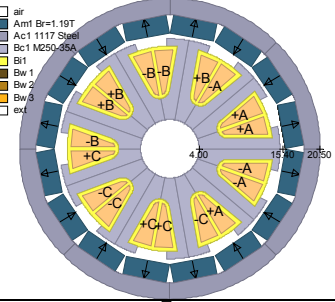
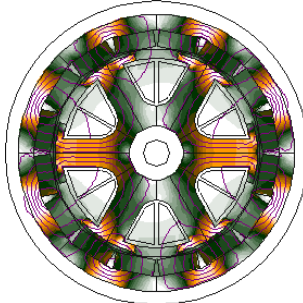
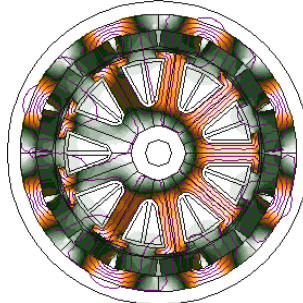
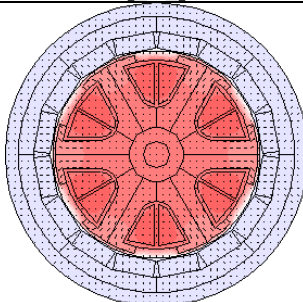
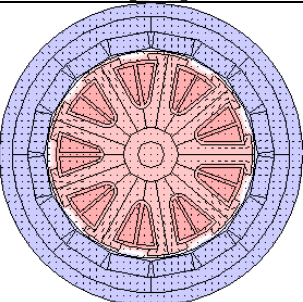
Figure 3.2 Proposed integration of an outer rotor permanent magnet (PM) brushless synchronous machine into a reduced harmonic gear unit

The specifications and the outcomes of integration and machine design are as following:

- Selection of gear unit: Size 17 ($\text{Ø}84, \text{H}36\text{mm}$) with ratio 50, 80, 100
 - Max input speed 10krpm, mean 6.5krpm, rated output speed 2krpm
 - Unknown no-load torque of the gear unit
 - Size 20 can reach up to 40Nm
- Selected available space for electrical machine $\text{Ø}41\text{mm}$ & $\text{H}26\text{mm}$
 - 8-pole rotor with surface mounted magnets NdFeB $6 \times 2.5 \times 26$ mm
 - 6 or 9-tooth stator with concentrated single tooth coils
- Electrical machine capable up to 0.2Nm i.e.
 - Current density 10 and 15 A/mm^2 , Power loss density 0.64 and 1.44 kW/dm^3
 - Torque capability at different current densities: 8p6s: 0.14 and 0.21 Nm vs 8p9s: 0.12 and 0.17 Nm
 - Shear stress up to 5200 N/m^2

Some outcomes from the machine calculations are presented in Table 3.2. In this table the layout of the machine is presented. The expected magnetic loading (0-2T) of the unloaded machine and the thermal loading (50-150 °C) at continuous operation at 10 A/mm^2 are presented.

Table 3.2 Calculation summary of the small PM machines for system integration

6-tooth 8-pole	9-tooth 8-pole	Remarks
		<p>Machine layout:</p> <ul style="list-style-type: none"> Outer rotor with surface mounted magnets 3-phase concentrated winding
		<p>Flux density distribution:</p> <ul style="list-style-type: none"> rotor: 2.2 - 2.5 T 8p6s: 1.6 and 1.6 T 8p9s: 1.8 and 1.9 T
		<p>Temperature distribution @h=15W/Km² and 40C</p> <ul style="list-style-type: none"> Hot-spot temperature, 8p6s: 134 and 251 C, 8p9s: 119 and 217 C Cooling surface, 8p6s: 93 and 160 C, 8p9s: 89 and 145 C

Summary, this study shows that the integration of special designed PM machine into harmonic gear is fully possible and this results a compact and lightweight solution. At the same time this solution seems rather costly when it comes to the cost of magnets in the machine and the gear components.

3.2 Magnetically deformed wave generator

Instead of taking advantage of tangential component of magnetic forces, which causes torque and rotates the wave generator or a rolling contact that deforms flex spline, the normal forces are used directly to deform the flex spline. Therefore the specific conception bases on direct magnetic wave generation (WG), that causes the attractive magnetic forces and thereby the deformation on the flex spline (FS) and formation of gear connection points. Expectedly the high (HI) speed magnetic wave rotation is transformed to low (LO) speed rotation of the flex spline (FS) due to strain wave gearing on the circular spline (CS). In order to take advantage of normal forces to deform the flex spline and form strain wave gearing the following questions need to be answered

- Dimensioning a flex spline for magnetic strain wave gearing
- Forces needed to overcome maintain the motion by redeformation of the flex spline

From normal magnetic forces point of view the air-gap flux density $B=0.7-1.0T$ causes magnetic stress tensor $\sigma=0.2-0.4MPa$ (Figure 3.3, left). These forces are used to deform the flexi cup (Figure 3.3, right) and the deformability depends on the dimensions and elasticity of the cup material. Depending on magnet arrangements, which is double or single excited, repulsive and attractive or only attractive forces are available, respectively.

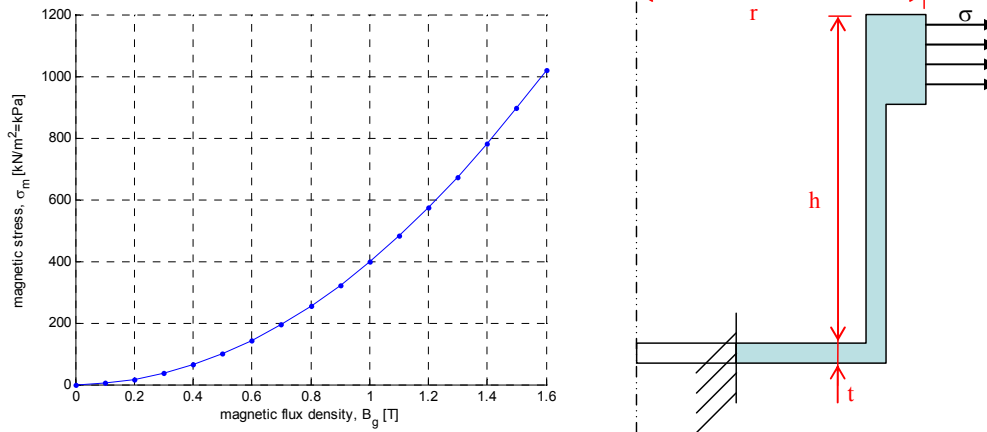


Figure 3.3 Magnetic shear stress as a function of flux density in the air-gap (left) and cross-section of a axisymmetric flex spline (right)

The rough dimensioning of the flex spline cup is based on 3D mechanic strain analysis and depends on dimensions (Figure 3.3, right) and material properties that are divided into 3 different groups:

- Low elasticity materials ($E=2\text{GPa}$) where are a number of thermoplastic polymers (polypropene, polyethylene, polystyrene, nylon)
- Medium elasticity materials ($E=20\text{GPa}$) where are a number of glass-reinforced plastics
- High elasticity materials ($E=200\text{GPa}$) where are a number of steel and iron compounds

Firstly, the analysis outcome of the **medium elasticity material** is shown (Figure 3.4). As the elasticity is low then the cup can have a smaller size or less force need to be applied to deform the cup. The cup is non metallic and therefore non-magnetic. This results an attractive solution for doubly magnetisation and FS arrangements with permanent magnets. Also single magnetisation is possible with a number of discrete magnetic pieces in FS cup that is used to create reluctance forces between the magnetiser and the FS cup.

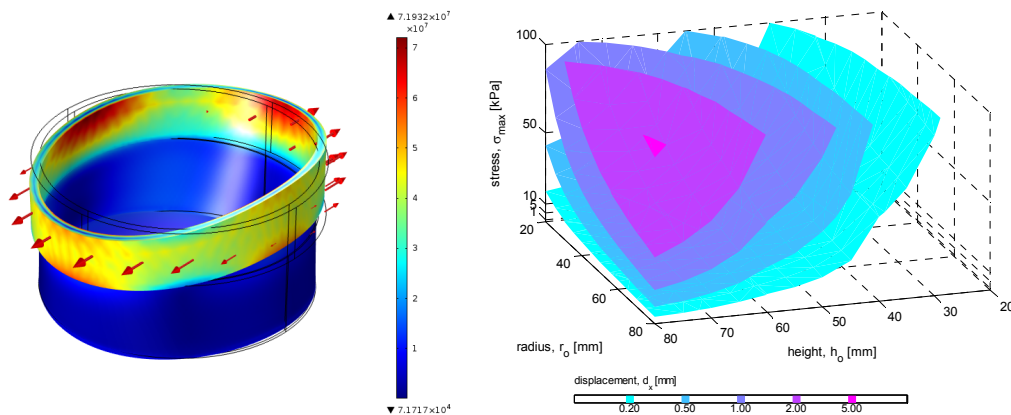


Figure 3.4 Image of von Mises stresses of the deformed medium elasticity (20GPa) cup (left) and maximum displacement as a function of applied stresses for a selected size.

In Figure 3.4 a FS cup with $R_o=50\text{mm}$, $H=50\text{mm}$ and 3 mm thick band has max displacement of 1.6mm and 0.08GPa von Mises stress @ diametrical stress distribution of 0.2MPa peak (0.7T).

Secondly, the analysis outcome of the high elasticity material is shown (Figure 3.5). As the elasticity is high then the cup should have a larger size or more force need to be applied to deform the cup. The cup is metallic and therefore can be magnetic. This results an attractive solution for single magnetisation where the FS cup operates for reluctance forces.

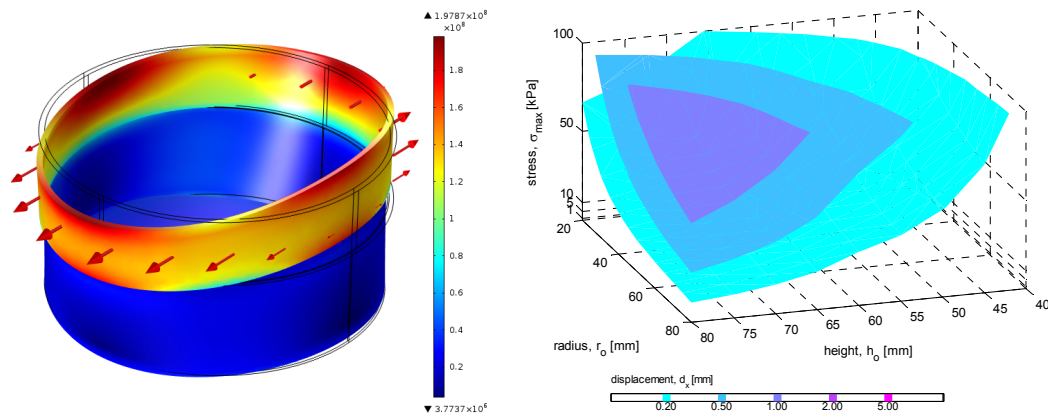


Figure 3.5 Image of von Mises stresses of the deformed high elasticity (200GPa) cup (left) and maximum displacement as a function of applied stresses for a selected size.

In Figure 3.5 a FS cup with $R_o=60$ mm, $H=60$ mm and 2 mm thick band has max displacement of 1.1 mm and 0.2 GPa von Mises stress @ diametrical stress distribution of 0.2 MPa peak (0.7 T).

Concerning the different selection options for the parts of magnetic strain wave gearing a number of topologies, which is in this case 8, are derived:

- Circular ring continuity – discrete sections vs complete single piece ring
- Flex spline location – inner or outer compared to the magnetiser
- Origin of magnetic forces – doubly excited magnetic type vs single excited reluctance type.

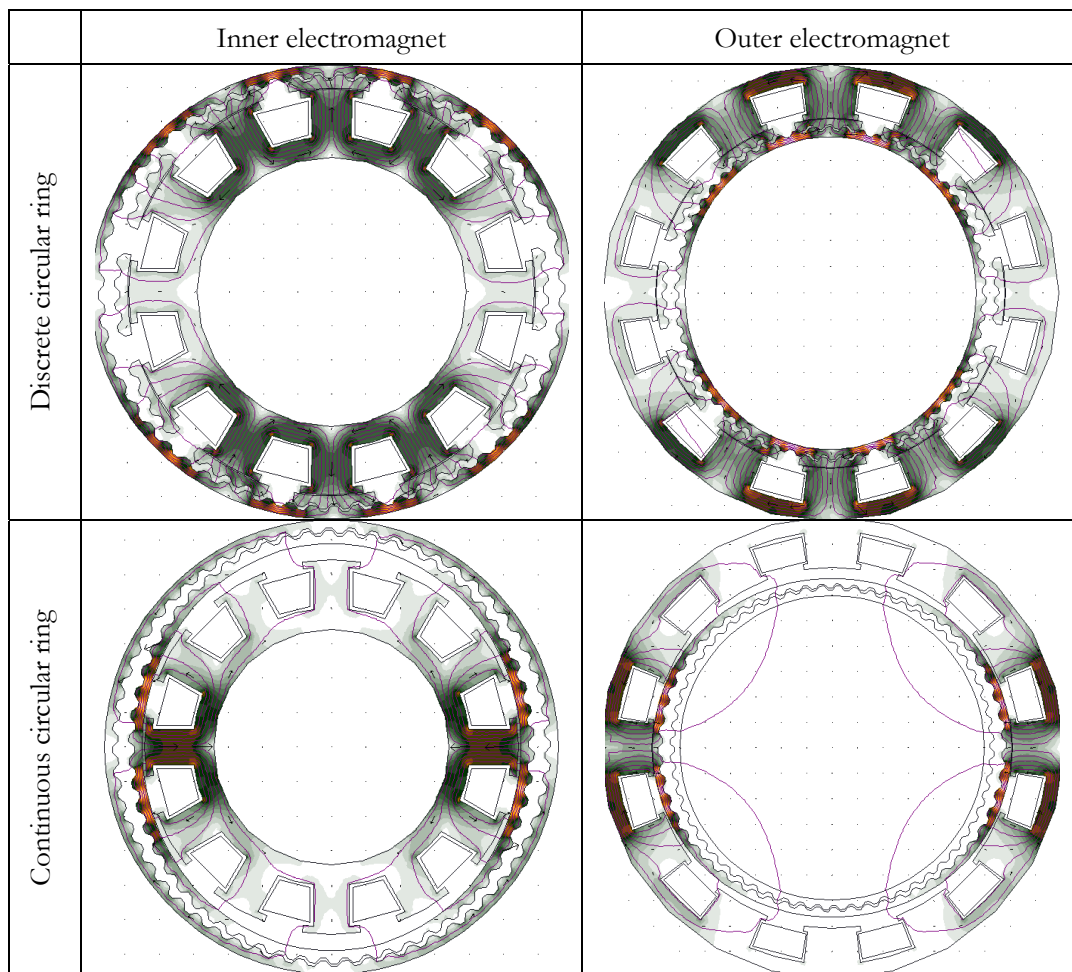
Four different configurations for reluctance type magnetic strain wave gearing actuator are shown in Table 3.3.

The finite element magnetostatic analysis of the integrated actuator is based on a mechanically deformed flex spline where the geometric reference is related to the previously calculated outer radius of the FS-cup (60 mm). The flex spline is defined similar to a cog belt with the intension of taking advantage of existing solutions for defining and trying out new ones. The harmonic transmission is initially defined as following:

- Flex spline: Maximum thickness 3 mm, tooth height 1.6 mm, number of teeth 58, maximum magnetic relative permeability of material ca 600.
- Circular spline: Maximum thickness 3 mm, tooth height 1.6 mm, number of teeth 60, maximum magnetic relative permeability of material ca 6000.

The aim of this analysis is to investigate magnetic flux density in the air-gap and in the flexi spline. Thin FS is easily deformable but it is not able to carry much flux without going into a deep saturation. Thick FS needs to accommodate more flux for higher flux density in order to apply more forces that are needed to apply for the thicker FS band. Force components are analyzed along the FS periphery. Moderately high current, which is 800 Atturns per coil, is applied in order to achieve reasonable flux density in the air gap and the flex spline. The maximum flux density in the air-gap is 0.7 T and more than 1 T in the flex spline. For sake of visualizing the actuator in action a series of simulations are made where the deformation and the excitation are rotated synchronously. The resulting simulation brings back to previously stated question on analysis of actual redeformation process and the most probable choice of materials for flex spline, which is preferably magnetic material for reluctance type of actuator and can be plastic and non-magnetic when comes to magnet type of actuator.

Table 3.3 different topologies of reluctance type for magnetic strain wave gearing



Magnet type of actuators can be derived similar way like reluctance type of harmonic gear integrated actuators (Table 3.3). One example is of PM excited actuator shown in Figure 3.6. The actual arrangement (Hallbach) and connection of permanent magnets ground more options for different solutions. At the same time the increased complexity restricts the further investigations on harmonic gear integrated actuators that operate on the principle of direct magnetic strain wave gearing based on the normal magnetic forces. The continuation of development in this direction could take significant advantage of harmonic gear producer or/and hands on study on that is based on existing components that can be used to form a strain wave gearing mechanism. In this case the usage of a cog belt is suggested in order to develop a strain wave gearing for practical concept evaluation and further development. Concerning to this suggestion some new ideas have appeared

- Magnetic cogs used for attraction
- RM or PM poles oriented and “used” axially or tangentially
- Stator tooth-tips as a part of mechanical gears
- Studying the advantages of transversal flux machine for deforming the cog belt or flex spline

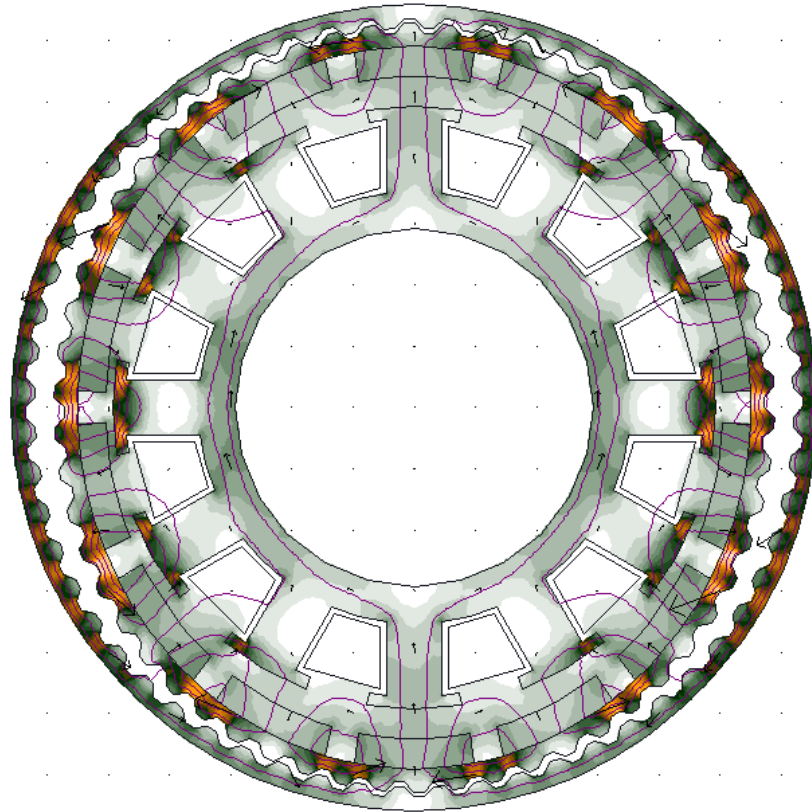


Figure 3.6 Inner electromagnet with PM excited flex spline and continuous circular spline

Summary, the experience from this study defines the hard contradictory specification for the flex spline that suppose to be thin in cross section to be flexible and easy to form strain wave gearing, simultaneously wide to carry the magnetic flux and strong to transmit the torque. The flexi spline can be designed directly for these purposes by separating the problem in multi-physics and conducting flux in transverse to spline direction instead of along the spline direction. This can lead to higher geometric complexity with different materials involved. Apart from that, the magnetic response of conducting in a magnetic conducting materials, huge air-gap and high force requirement are not the stimulating features that need to find intelligent solution.

4 A cycloid gear integrated into an electrical machine

Similar to harmonic gear the cycloid gear makes high gear ratio possible. The advantageous features for cycloid drive is that the unit can be thinner and more efficient compared to the corresponding harmonic gears. The drawbacks are a larger gear ratio ripple and backlash. Also according to [11] the cycloid gear can not meet the maximum gear ratio for the matching harmonic drive.

Two different electromagnetic integrations of cycloid gears are considered:

1. “low number of cogs” rolling contact hypocycloid gear
2. “high number of cogs” eccentric friction transmission

During the course of project the starting point is a full integration of the magnetic clogged cycloid while the experimental orientation has conducted the research towards electromagnet friction cycloid. As an outcome the reduction of complexity of a clogged electromagnetic cycloid gear has met the rapid prototype of a frictional electromagnetic cycloid gear.

4.1 Electromagnetic clogged cycloid

The speed reduction of a cycloid gear bases on the incoming forced eccentricity via the rolling contact between a cycloid gear lobes and a ring gear to the output axel. As an outcome the forces of the input eccentric axel rotate and translate the cycloid disk in respect to the rollers of the stationary ring. This results speed reduction from the input speed down to rotation of the cycloid disk. The eccentric translation of the cycloid disk is taken care by pin transmission to output disk or an Oldham coupling of unaligned axes. The transmission ratio is related to number of lobes N_L on a cycloidal disk and number of rollers N_R of a ring gear, where the number of lobes is one less than number of rollers.

$$ratio = \frac{N_R - N_L}{N_L} = \frac{1}{N_L} \quad 4.1$$

In this electromagnetic rolling cycloid the following integration steps are suggested:

1. the rotating eccentric input from the electrical machine to the cycloid disk is replaced with electromagnet that forces the cycloid disk directly
2. the rollers of the ring gear is part of magnetizer or more or less a conventional machine stator

The integration resulted to a 12-coil magnetizer that can integrate easily $N_L/N_R=11/12$, $23/24$ or $35/36$ reduction hypocycloid gear. Figure 4.1 shows these different configurations at loaded condition. The forces at Figure 4.1 is calculated at the “zero” rotor position, where the rotor is the farthestmost along x-axis, and phase B is excited with 7.5 Amps.

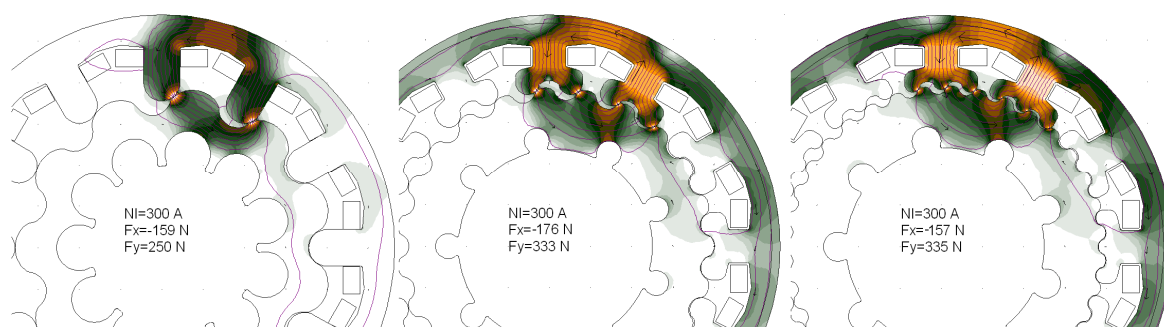


Figure 4.1 Rotor is located farthestmost right along x-axis and this defines position at 0 degrees. Coil excitation at 60 and 90 degrees results 75 degrees. The resulting force vectors are 122, 118 and 115 degrees for 11/12, 23/24 and 35/36-cog rotors, respectively.

Design of a cycloid gear

A design tool for clycloid gear based on epitrochoid trace has been developed by Bengt Cyrén. This tool is used not only to select eccentricity and specify the main dimensions for the gears but also to visualize the force action in the system. The mechanical friction and tolerances can be accounted in order to make the task complete for practical realization. The main concern on the force analysis has

been the actual outcome of the forced system: applied forces from electromagnetics vs reaction forces from the gear unit (Figure 4.2).

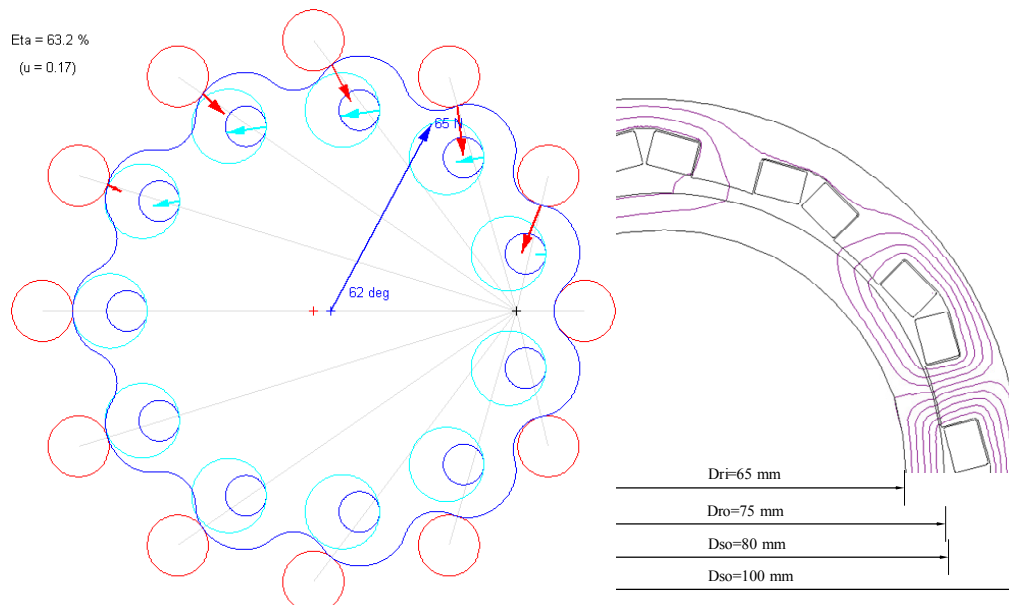


Figure 4.2 Left: force analysis on a cycloid gear producing 1Nm on output shaft where the roller center radius (R_{40}) merges the inner diameter of stator and the difference between the diameters (rotor and stator) has defined the eccentricity of 2.5 mm. Right: the initial analysis of an electromagnet with a rolling rotor.

Figure 4.2 shows the desired direction and magnitude for the applied force (1:00 o'clock) in order to produce 1 Nm of torque on the output shaft when the cycloid is located far most along x-axis (3:00 o'clock) and the friction is 0.17. Ideally, with no friction, the corresponding force magnitude is 45 N at 54 degrees. Obviously the force demand per unit of torque can be reduced by increasing the eccentricity or by increasing the number of rollers. From integration point of view the direction of the applied magnetic force co-aligns with the reaction forces as in these connection points the air-gap is the smallest and flux density is the highest, unless if this is regulated by magnetic saturation.

From this point it is not obvious at all whether this device comes to action or rather locks itself by the applied electromagnetic forces. As an outcome a few different layouts has been tested for redirecting the action of magnetic forces for collaborating with the gearing forces. For sake of this challenge the magnetic actuation has later been separated from mechanical transmission in order to get better understanding of the integration consequences.

Analysis of magnetic forces

As an outcome of the mechanic integration it has been important to study the static forces and kinematics of the proposed magnetic actuator. By starting from the mechanical transmission in action the conventional cycloid drive have input and output that move in opposite direction. The magnetization cycle is selected to move in counter clock direction and so do the cycloid disk in a series of magnetostatic simulations. This selection can be understood as a contradiction to opposite direction but this is based to magnetic action to attract the magnetized bodies in the direction of the magnetic field. The series of magnetostatic analyses are specified as

- At 10 rotor positions from 0 to 90 degrees with step of 10 degrees
- At 6 combinations of coil excitations: 1) 3 o'clock – A, 2) 2:30 – A+B, 3) 2:00 – B, 4) 1:30 B+C, 5) 1:00 – C and 6) 0:30 – C+D, and
- At 3 levels of currents: 1, 2 and 3 which corresponds to 2.5, 5 and 7.5 Amps.
- The stator is specified as 114*0.35 mm M250-35A and 40*0.9 mm copper wire in the CAD coil cross-section of 27.7 mm².

The simultaneous rotation of magnetic excitation together with rotation and translation of cycloid disk results the resultant applied force and force angle according to Figure 4.3, which is calculated for the 35/36-cycloid.

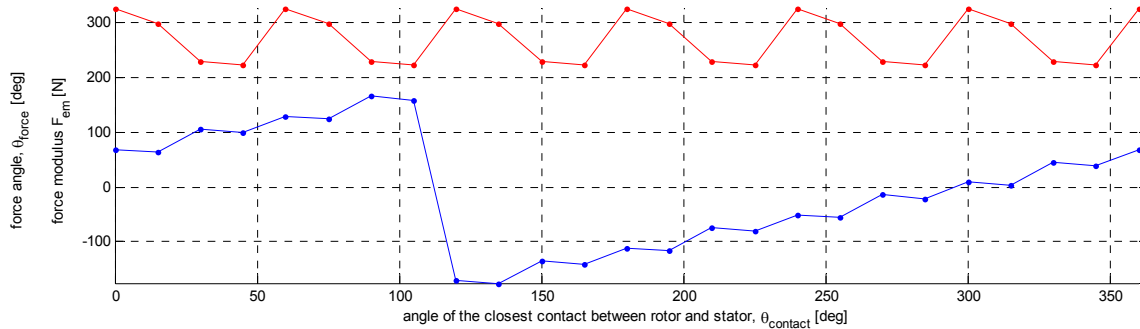


Figure 4.3 The excitation cycle: $0 \leq \theta_{\text{rot}} < 30 \rightarrow A+B$, $30 \leq \theta_{\text{rot}} < 60 \rightarrow B$, $60 \leq \theta_{\text{rot}} < 90 \rightarrow B+C$, and so on, results the force modulus (red line) and the force angle (blue line)

The forces at Figure 4.3 is taken at the rotor positions of 0 and 14.4 at 5 Amps A+B, rotor position 28.8 and 43.2 at 5 Amps B, 57.6 and 72.0 at 2 Amps B+C, and so forth and on.

The forces at Table 4.1 (like in Figure 4.1) is calculated at the “zero” rotor position, where the rotor is the farthestmost along x-axis, and phase B is excited with 7.5 Amps. When following the excitation sequence A, A+B, B, and so forth and then the resulting force vector is already in the second quadrant when the excitation coils are in the “first quadrant” (Table 4.1).

Table 4.1 Electromagnetic forces applied on the different rotors depending on coil excitation

Excited coils	A		A+B		B		B+C		C		C+D	
	F_x	F_y	F_x	F_y	F_x	F_y	F_x	F_y	F_x	F_y	F_x	F_y
11/12-cog 0.1-gap	312.0	203.7	151.6	458.6	-159.2	250.3	-466.5	384.0	-306.7	133.5	-647.1	87.2
23/24-cog 0.1-gap	260.4	137.2	81.4	474.7	-176.9	333.4	-612.5	523.2	-432.1	187.9	-916.8	122.1
35/36-cog 0.1-gap	259.1	117.5	100.4	454.8	-157.4	335.2	-615.1	533.4	-458.7	200.3	-971.5	129.3
11/12-cog 0.03-gap	382.0	201.4	264.4	394.0	-115.9	188.6	-307.0	271.5	-191.1	83.1	-394.2	55.2
23/24-cog 0.03-gap	327.6	126.5	204.9	392.5	-119.2	262.0	-393.8	382.8	-270.0	117.9	-569.9	78.5
35/36-cog 0.03-gap	335.6	104.7	234.5	374.3	-98.8	267.8	-407.9	403.4	-309.0	136.7	-647.7	89.6

The process of force calculation is following: Force components F_x and F_y that are applied to the rotor are calculated from the magnetic field distribution between the rotor and the stator. Rotor is rotated and displaced to have predetermined closest distance between the stator and rotor. The predefined distance is 0.1 and 0.03 mm. This distance prevents the geometrical overlap and leaves small non-magnetic gap so that the magnetic forces can be calculated. The calculation domain is whole rotor revolution and 6 different combinations of excitations at different current levels. Figure 4.4 shows the fraction of the calculation results. These magnetic forces F_x and F_y are the outcome of the phase B excitation at 7.5A and the rotor rotation of 90 degrees. F_n is the modulus of the force, F_r is the radial component of the forces that try to attract the rotor and F_t that try tangential forces to displace the rotor at 75 degrees (which is the magnetization direction for phase B).

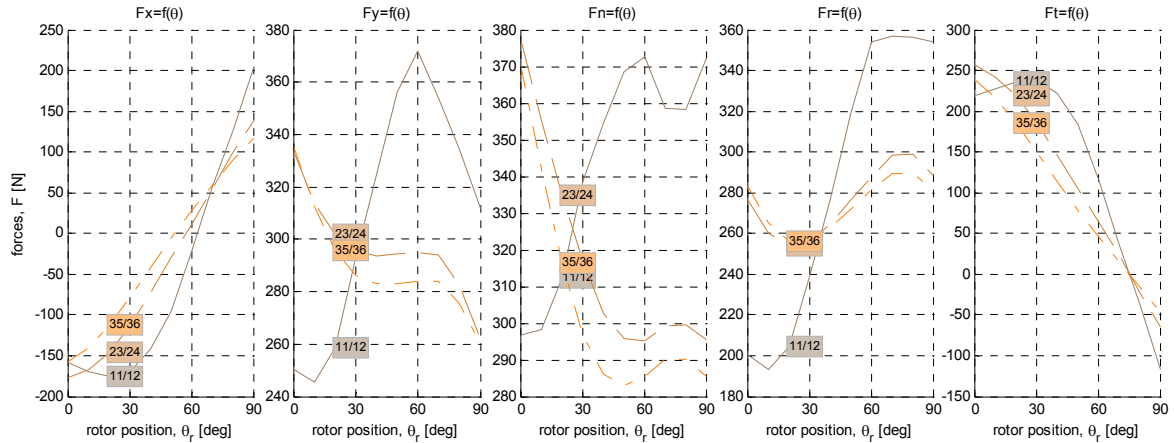


Figure 4.4 Forces applied to the rotor as a function of rotor position. These forces are due to the magnetisation of phase B of 300 Ampere turns

The resultant forces are plotted in stator coordinate system (Figure 4.5, left) so that the locus of the resulting forces as a function of rotor position (Figure 4.5 left) is seen. This resulting force can be divided into two components (Figure 4.5 right) where the radial force shows that the excited coil tries always attract the rotor and the tangential shows the capability to drag the rotor into the alignment.

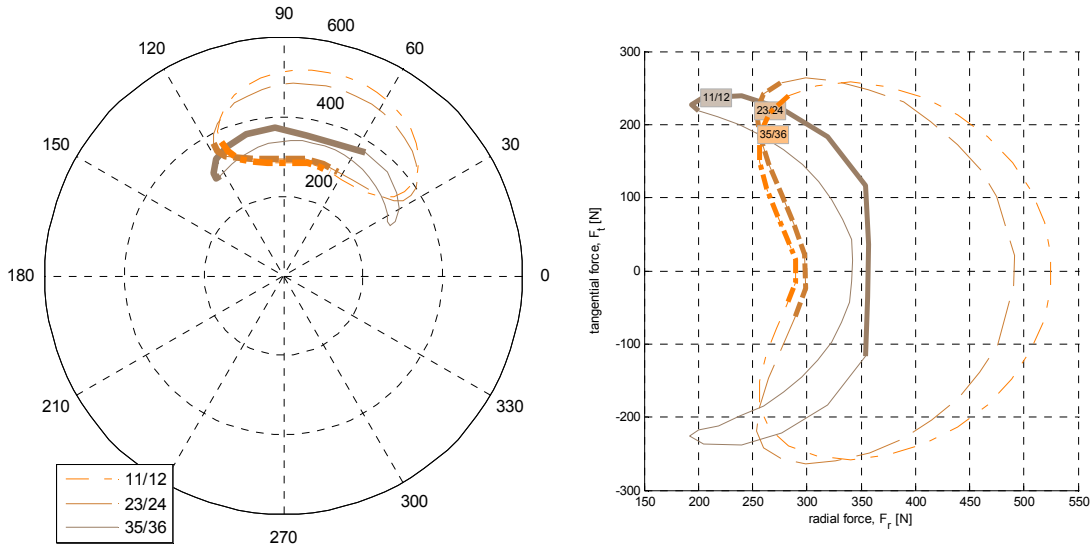


Figure 4.5 The locus of the resulting magnetic forces as a function of rotor position when phase B is energised (left). Radial and tangential force components in the resulting magnetisation direction (right). Bold lines show the first quarter of rotation (0-90 degrees).

The electromagnetic torque is related to nearly the tangential forces applied to the radius of 38 to 40 mm. The resultant electromagnetic torque is also calculated from the field values between the stator and the rotor (Figure 4.5). 0.1 mm distance is considered at the alignment.

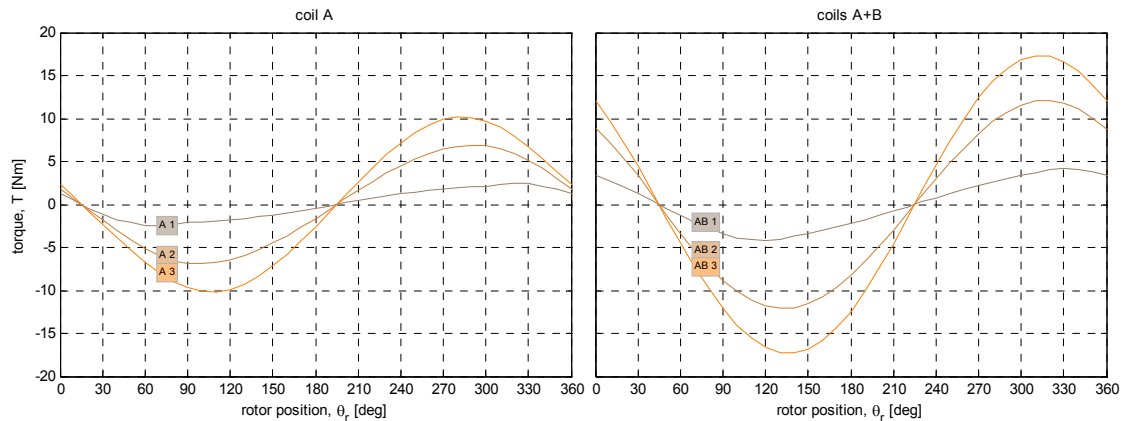


Figure 4.6 The locus of the resulting magnetic forces as a function of rotor position when phase B is energised (left). Radial and tangential force components in the resulting magnetisation direction (right). Bold lines show the first quarter of rotation (0-90 degrees).

Considerations related to the actual “air-gap” distance between the stator and the rotor

1. In reality the air-gap between the stator and rotor is minimized to zero due the magnetic forces
2. For practical reasons a small air-gap is present in the FE model for magnetic calculations, this can be as small as 1pm (1e-12 m) or even less until the feasible solution can be obtained: non-overlapping geometries, reasonable amount of finite elements and so on
3. There are two specific features to the outcome of the actuator parameters when rotor is moved towards tighter contact to the stator
 - a. Magnetic saturation becomes dominating, force capability becomes actually lower at higher currents but not lower excitation currents
 - b. The air-gap in the opposite side of the “connected” surfaces becomes larger and the high forces due to local high field and flux density disappear

The analysis of the 11/12, 23/24 and 35/36 cog arrangement have following outcomes

1. The electromagnetic forces are rather unchanged and have small influence on the layout of the reluctance rotor
2. It is expected that the cogs require more radial spacing due to higher cog radii
3. It is expected that the core losses are changing with the selected configuration and this is shown on Figure 4.7. The electric frequency is selected $1/(1-N_{cr}/N_{cs})$ higher from the mechanical frequency of the output shaft. The magnetisation frequency is 6 times higher than the electric frequency and the duty ratio is 1/6.

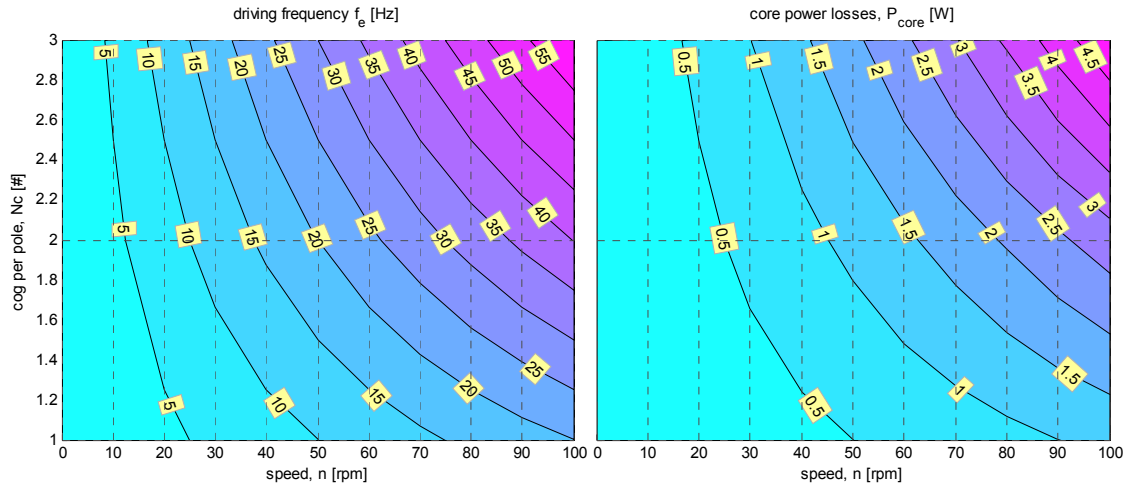


Figure 4.7 driving (electric frequency) and the rough estimate of the power losses in the core

Summary, a complete magnetostatic FE analysis is carried out where, forces (x, y, radial, tangential, modulus, angle), torque and flux linkage at each coil, and flux density in the core are obtained as a function of cycloid disk position and distance from the stator, currents alone and in combinations. Further on the flux density matrix is used to obtain core losses at different operation points.

$$[\mathbf{F}, T, \boldsymbol{\psi}, \mathbf{B}] = f(\theta, d, \mathbf{I}(\theta)) \quad 4.2$$

This complete map of information is calculated for a number of different actuators. Anyhow the complete model in simulink, where the electromagnetic actuation is connected to mechanic transmission, is not completed to the end and therefore the outcome of this actuator characterization becomes incomplete from system realization point of view. Anyhow the expectation that the actuator forces locks up with the reactions from the mechanical transmission has stopped the system model development.

CAD for prototyping

The production files are finalised for 35/36 electromagnetic cycloid and the cross-section view of the CAD is shown in Figure 4.8.

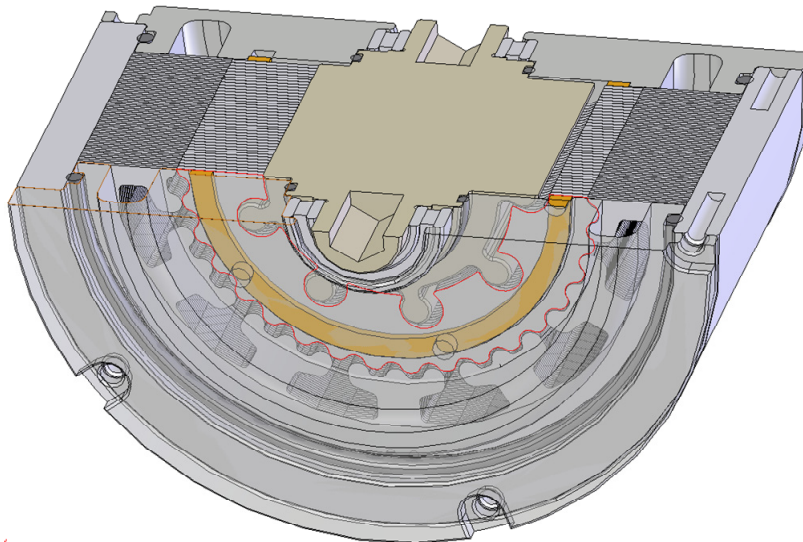


Figure 4.8 Section view of the cad drawing

4.2 Electromagnetic friction cycloid

Frictional EMCD is proposed due to simplicity and chance for rapid prototyping together with learning activities when merging the transmission into an actuator. This prototype uses an exciting stator from the BEVI and a piece of solid ferrous tube for the rotor. This rapid prototype could facilitate

- Concentrated winding development for high specification requirement and feasible production
- Analyze the forces related to the excitation sequence
- Development of control strategy and topology until the realizable solution

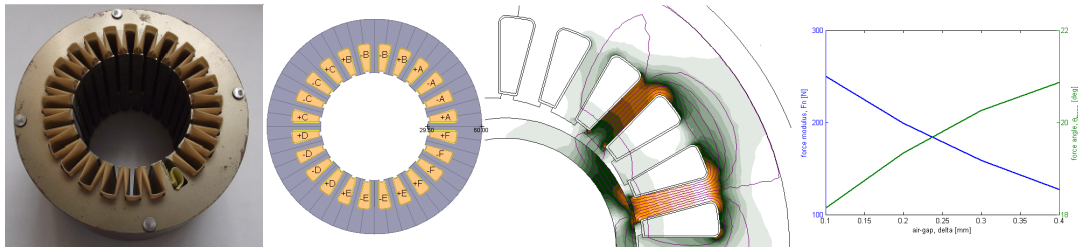


Figure 4.9 Presentation of the proposed rapid prototype

Rough analysis of magnetic forces are done for M700-50A core and coils that carry 400 Amp turns, which in current configuration is relatively demanding: 50% fill factor inside the insulated slot with 0.35 mm insulation and 10 A/mm² current in the wires.

The electromagnetic action to the transmission that is supported from the connection point A results torque on the output shaft (Figure 4.10) and is calculated according to

$$T_{drive} = \sum_1^{\#coils} F_{my} R_3 (1 - \cos(\alpha)) + F_{mx} R_3 \sin(\alpha) \tag{4.3}$$

where α is the resulting applied magnetic force angle and the force components (F_{mx} and F_{my}) are calculated from FEM. Depending on the rolling gear, whether it is the same as the rotor in a stator ($R_3=R_1$) or it is separated from electromagnetics and can be considerably larger, more torque can be transferred from the produced electromagnetic forces.

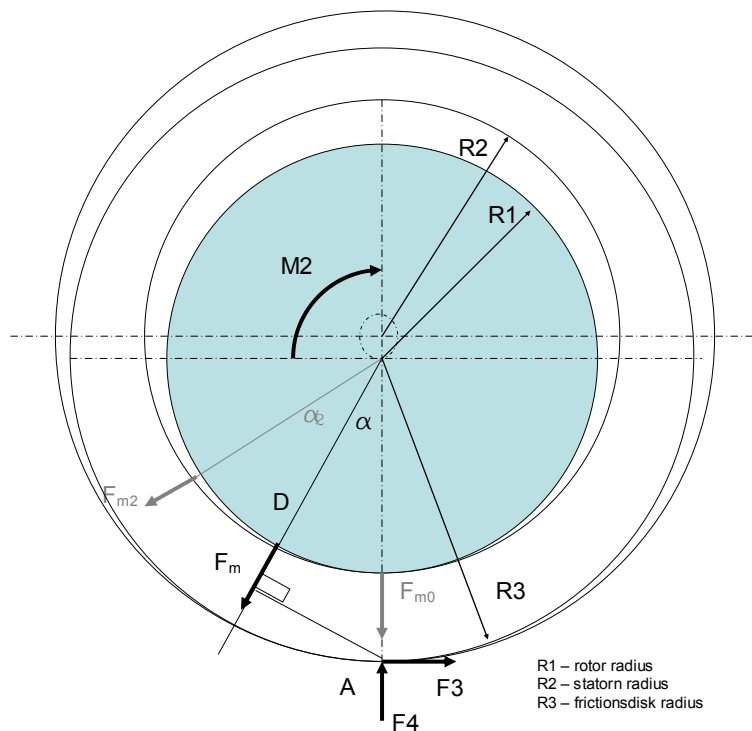


Figure 4.10 Force diagram in a cycloid gear

This analysis tool for the mechanical forces in a frictional cycloid transmission is developed by Thomas Rundqvist. In this case the electromagnetic force per coil is represented as a function of air-gap: $F_m = 257.96e^{2.43g}$, which is in accordance to the FE simulations at 6 A per coil. These forces are distributed around the periphery depending on how many of the coils are energized. The output torque is related to the applied magnetic forces in respect to the connection point A. The capability to produce torque depends not only on the electromagnets to create magnetic forces but also on the mechanics whether the connection point can be kept on the place to transmit the torque. This is calculated according to

$$T_{hold} = R_3 \mu \left(F_{m0} + \sum_1^{\#coils} F_m \cos(\alpha) \right) \quad 4.4$$

The radial force component F_{m0} is the initial vertical force that establishes the connection and makes the transmission possible. As the forces cause motion the magnitude of the driving and holding force and torque depends on rotor position and the character is repeated as many coils are around the periphery plus the character of the gravity forces.

The outcome of the analysis tool is presented later in the experimental section. Before that the analysis of rolling electromagnet are shown and the basis for the prototype presented.

Electromagnetic redesign

Based on the early practical experience from the rapid prototype a redesign process is introduced. The existing prototype (Pro-1) consists of 1) a complete 12-coil stator (core $D_o/D_r-H=120/60-75$ mm + coils $H_w=130$ mm) and 2) provisional roller (rotor) core. The missing parts are 1) redesigned roller (rotor) core, 2) friction transmission rings, 3) end-plates and 4) Oldham coupling, which is not drawn in Figure 4.11. The drawing shows some proposed stators for a new EMCD prototype (Pro-2), which are either specially designed for a higher magnetic loading or selected among standard stator laminations. Figure 4.11 shows also two possibilities for the separated mechanical transmission from the electromagnetic actuator.

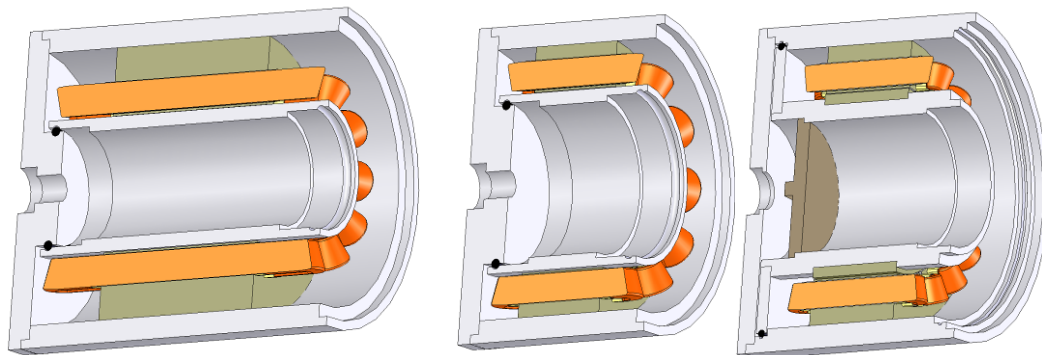


Figure 4.11 Partly ready prototype (left) and suggestions for new prototypes under discussion (right)

Design targets

Design is a compromise. The current situation of the design development is influenced by a choosing among these three key factors: a concept demonstrator, a completion of application requirements and a reasonable cost of the prototype. In the perfect case the design is easily realizable, demonstrates the expectations on functionality and meets or exceeds the requirements. Practically the realization time and cost can be significantly improved by selecting among exciting components rather than reinventing, optimizing, developing and producing somewhat improved components. The design adaption, concept scalability, rapid prototyping and evaluation are becoming the powerful input to topology development and optimization. As an outcome of this background there are three design approaches and the stator designs are shown accordingly (Figure 4.12). The stator topology overview is shown in Table 4.2.

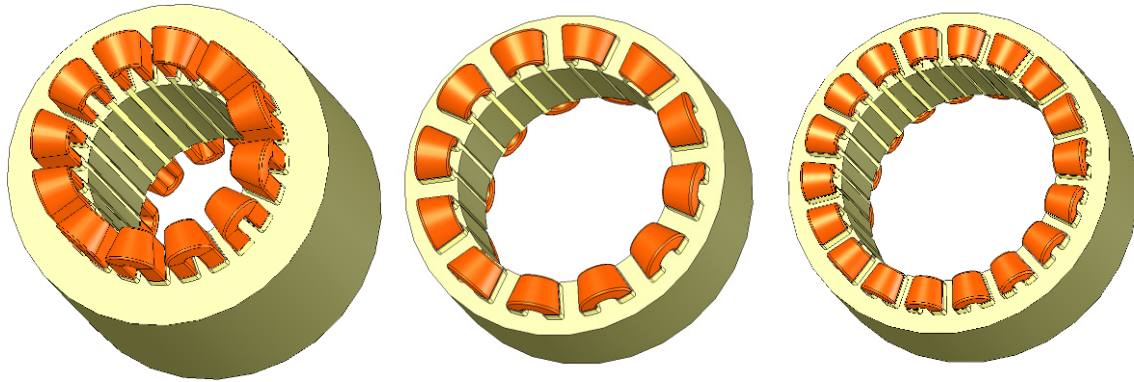


Figure 4.12 Design targets: initial prototype stator (left), optimised design (middle), and easily realizable design (right)

Table 4.2 overview of suggested prototypes for stator

	Early prototype (Pro-1)	Optimized (Pro-2a)	Easily produced (Pro2b)
Stator core, Do/Di-H [mm]	120/60-75	120/60-40	120/80-40
Axial height of windings	130	60	65
Advantages	prototyped stator and windings Easily evaluated for model improvement	special stator is designed	existing stator core Adjustable axial height
Disadvantages	long core & end-turns non-optimal core	significant production time and cost	non optimal core

Electromagnetic and heat transfer analysis

A few FE analyses are made in order to specify the EMCD unit and obtain the characteristics of the device. The roller/rotor diameter is selected 1 mm smaller than the inner diameter of the stator. The magnetic core is selected the same for the stator and rotor, and this varies between the different design targets. The thickness of the main insulation is selected 0.35 mm. The magnetizing current (6 Amps) is selected the same for the different target designs. This means that the smaller slots accommodate the same number of turns, although smaller diameters, which carry the same current but is loaded by higher current density. The initial calculation is carried out for the roller/rotor that is centered and has equal air-gap of 0.5 mm. The EMCD unit specification is shown in Table 4.3.

Table 4.3 Prototype specification

	Early prototype	Optimized	Easily produced
Active length, L_a [mm]	75	40	40
Core material	M700-50A	M330-30A	M330-30A
Number of slots	24	24	36
Slot area, A_s [mm ²]	87.2	75.6	53.2
Winding area, A_w [mm ²]	73.0	62.8	42.3
Parallel strands x number of turns, $N_c \times N_t$	2x45	2*45	1x45
Conductor diameter, d_c [mm]	0.71	0.65	0.75
Fill factor, K_f [%]	48.8	47.6	47.0
Current, I [A]	6	6	6
Total current, I_N [Aturns]	270	270	270
Current density, J [A/mm ²]	7.58	9.04	13.6

The electromagnetic analysis is made at one coil excited (index 1 in Table 4.4) and two coils excited (index 2 in Table 4.4). The rotor is centered and is forced horizontally (F_x) if one coil is excited. With the two coil excitation both horizontal (F_x) and vertical forces (F_y) are applied.

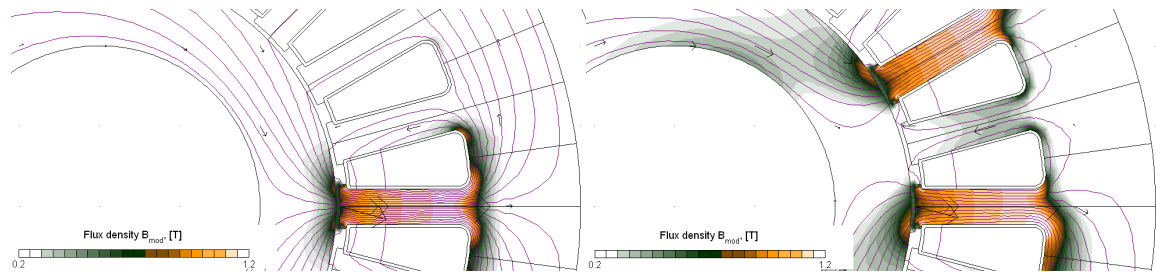


Figure 4.13 Pro-1 with one coil excited (left) and two coils excited (right). The excitation current is 6 Amps.

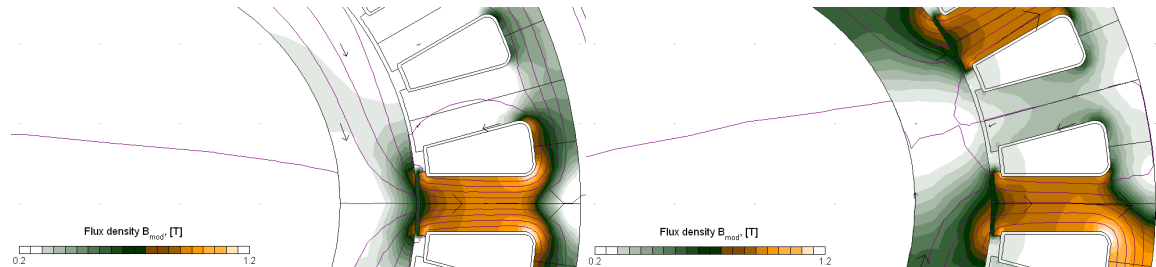


Figure 4.14 Pro-2a with one coil excited (left) and two coils excited (right). The excitation current is 6 Amps.

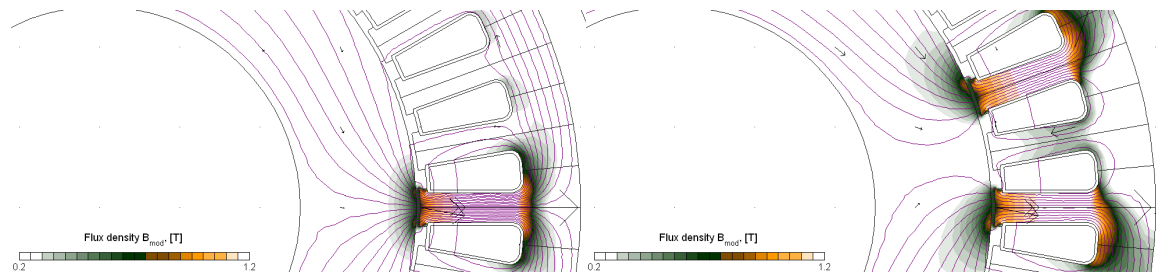


Figure 4.15 Pro-2b with one coil excited (left) and two coils excited (right). The excitation current is 6 Amps.

The results of the magnetic calculations are obtained over the active part of the actuator. This means that the end turn inductance and resistance are excluded in this calculation. The results are presented in Table 4.4

Table 4.4 Magnetic fluxes and forces at 6 A current per coil

	Early prototype	Optimized	Easily produced
Voltage Drop, U_r [V]	0.895	0.561	0.843
Flux Linkage, Ψ_{i1} [mVs]	16.7	11.5	8.12
Flux/Current, L [mH]	2.78	1.92	1.35
Voltage/Current, R [Ohm]	0.149	0.123	0.199
Power Drop, P_r [W]	5.37	3.36	5.05
Gap flux density, B_{gm} [T]	0.65	0.63	0.64
Electromagnetic forces, F_1 [N]	65.9 + j0	51.4	32.5+j0
Flux Linkage, Ψ_{i2} [mVs]	16.0	10.9	7.91
Electromagnetic forces, F_2 [N]	111.1+j29.8	86.2+j23.1	58.9+j10.2

The thermal model is defined as following:

- Natural cooling conditions from the radial outer surface of the stator housing: $h=15$ W/Km², $\vartheta_{amb}=40^\circ\text{C}$
- Thermal conductivity of core, main insulation and winding are: $\lambda_{core}=36$ W/mK, $\lambda_{ins}=0.12$ W/mK, $\lambda_{win}=0.3$ W/mK,

The outcomes of the steady state heat transfer analysis are presented in Figure 4.16 and Table 4.5.

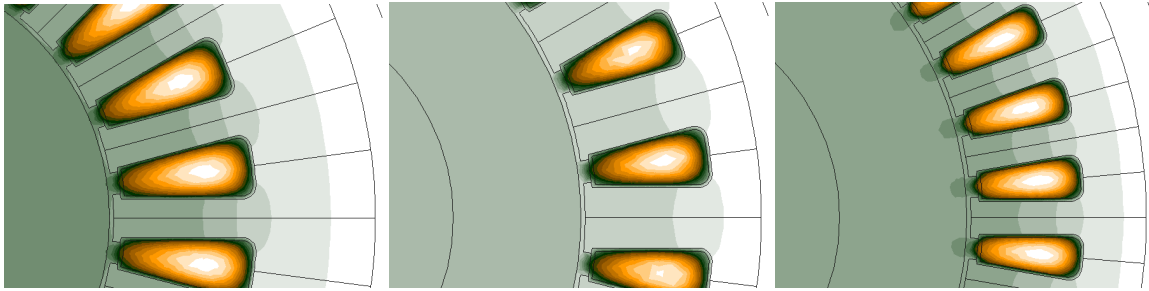


Figure 4.16 Temperature distribution of Pro-1 (left), Pro-2a (middle) and Pro-2b (right). The minimum and maximum values of the temperature scale are the housing surface and the hot-spot temperature of the winding.

Table 4.5 Power losses at 6 A current per coil and temperature at steady state

	Early prototype	Optimized	Easily produced
Power loss density, Q [kW/m ³]	490	670	1493
Maximum temperature, ϑ_{\max} [°C]	191	217	432
Surface temperature, ϑ_{surf} [°C]	180	205	412

Actuator characteristics

The magnetic flux, force and torque maps are calculated as a function of combination of coil excitation, current magnitude and rotor position. Three low speed force capability of three different candidates for the prototypes are plotted in Figure 4.17.

- Excitation is defined between 0 and 60 degrees, either 3 (24-slots) or 4 (36-slots) coils lighted
- Current is changed in four steps: 3, 5, 7 and 9 Amps
- The rotor is moved along a line – a displacement line. This line is defined as a distance between stator and rotor, which is changed from 50 μm to 950 μm i.e. from 0% to 100%.

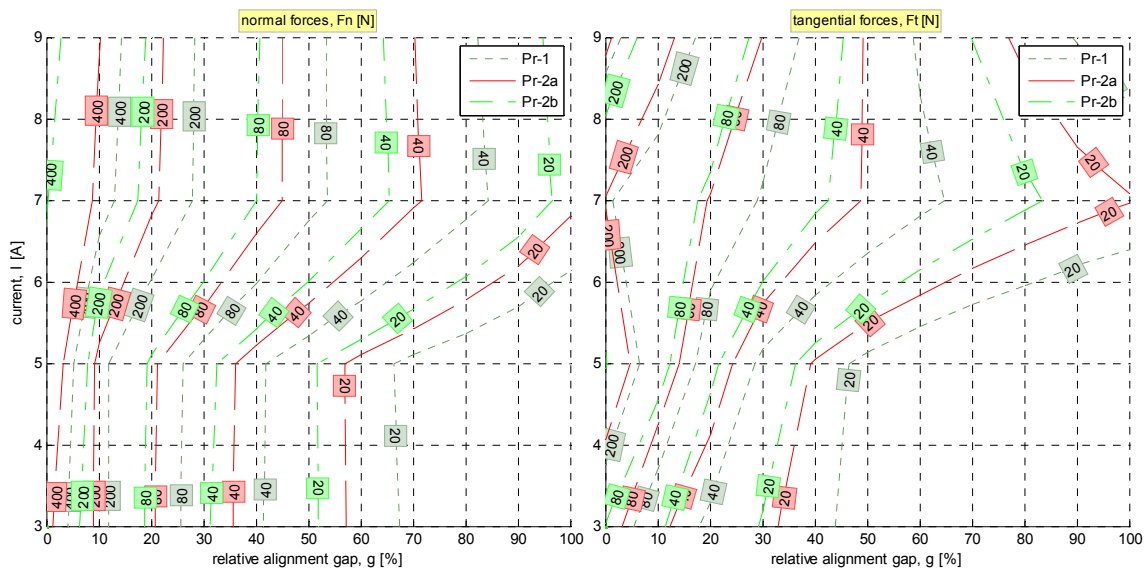


Figure 4.17 Force comparison of Pro-1 (left), Pro-2a (middle) and Pro-2b (right).

Following observations are made

- Pro-1 (Pr-1) 24-slots 75 mm existing prototype can provide most force normal and tangential for given current and gap.
- Pro-2b (Pr-2b) 36-slots 40 mm easily manufactured prototype suffers under the thermal and magnetic limitations of excessive heat losses and magnetic saturation.

- For the same thermal constraints the Pro-2a current of 6A has to be reduced $\sqrt{217/432}$ times that according to present normal force ratio of 302/436 and tangential force ratio 360/436 at the minimum air-gap results that Pro-2b is able to provide 49% of the normal forces and 58% of the tangential forces that the optimized Pro-2a could provide at the same circumstances.

Conclusions after the current analysis

- Pro-1 is probably the best when it comes not only to force capability and the realization in terms of speed and cost but also the chance to show the functionality of the concept. The obvious drawbacks are that 1) the size is far from the application requirements, 2) the suggested solid rotor limits the performance, 3) the transmission implementation prefers small -transmission-diameter
- Optimized Pro-2a has good chance to over perform easily realizable Pro-2b, still there is additional cost of finalizing the design, producing the parts and assembling them, which increase the realization in terms of speed and cost and likely it would not clearly outstanding than Pro-1.

Prototyped electromagnetic actuator

The new prototype of electromagnetic actuator, which is built by BEVI, consists of

- laminated 24-slot stator with 12 coils (core Do/Di-H=120/60-75 mm + coils Hw=113 mm)
- laminated rolling rotor (core Do/Di-H=59/30-75 mm)

The stator model is built according to built prototype. In this model a constant width of 4 mm for the stator teeth is assumed. The inner radius for the yoke is (R_y) 75 mm. The geometric data varies slightly from the CAD for prototype where the corresponding numbers are 4.07-4.32 mm and 76 mm, respectively. The actual axial length for the coils is taken 113 mm ($97+2 \times 8$) according to the CAD drawing and the geometric outcome of the 3D model is shown in Figure 4.18. The core material is (expectedly) M700-50A and the rest of stator specification is Table 4.6 It is assumed the same magnetic properties for the rotor lamination are nearly the same as for the stator. The theoretical expectations of the stator are already presented under “Early prototype” design. The (CAD) estimated volume of the displaceable rotor parts (excluding small details) is 0.35 dm^3 that with average mass density of 7.5 g/dm^3 gives the weight of 2.6 kg

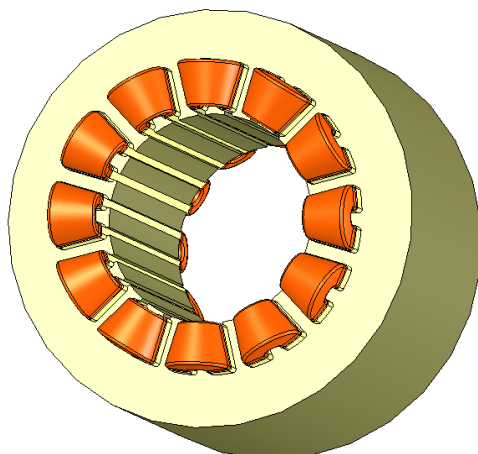


Figure 4.18 The 3D geometric stator presentation used in 2D FE simulations

Table 4.6 Prototype specification

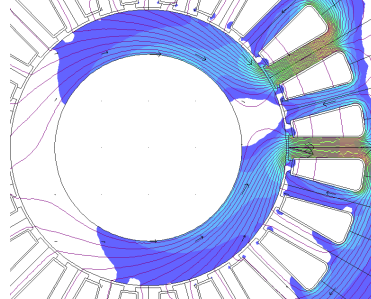
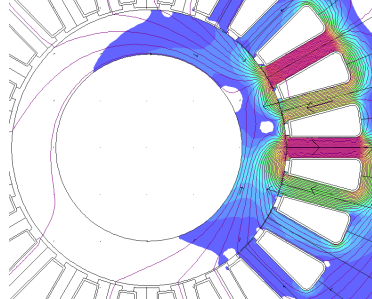
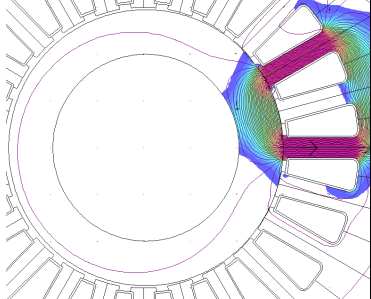
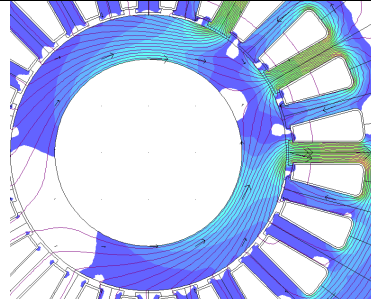
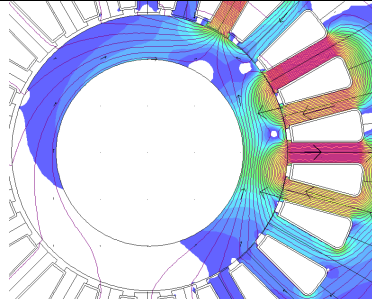
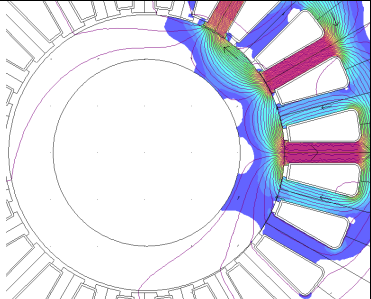
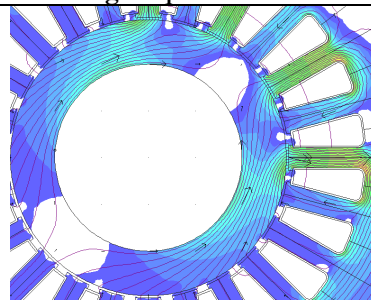
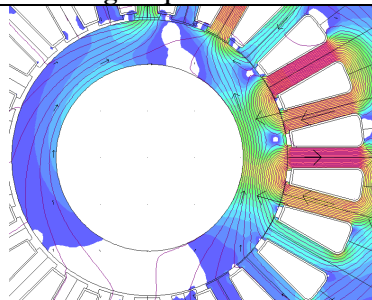
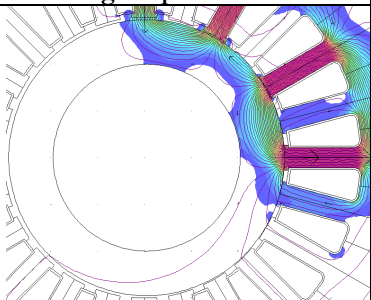
Dimension and unit	value
Active/actual length, L_e/L_a [mm]	75/113
Number of slots	24
Slot area, A_s [mm ²]	87.2
Winding area, A_w [mm ²]	73.0
Linter thickness, d_i [mm]	0.35
Parallel strands x number of turns, $N_c \times N_t$	2×45
Conductor diameter, d_c [mm]	0.71
Fill factor, K_f [%]	48.8
Current, I [A]	6
Total current, I_N [Aturns]	270
Current density, J [A/mm ²]	7.58

FEM Model used to calculate the force and torque according to following specifications

- Excitation current 6 Amps corresponds to 7.5 A/mm^2 in wire
- Rotor location. A) centered, B) moved to the right $4.9\text{e-}4$, air-gap $10\mu\text{m}$
- Magnetization direction of magnetized teeth: A) homopolar B) bipolar
- Excitation of coils: A) 2-3, B) 1-2-3, C) 12-1-2-3
- Resultant direction of magnetic forces: A) 15 deg, B) 45 deg, C) 60 deg

The driving torque (Table 4.7) is the maximum value of the expected torque according to equation 4.3 at the force components of magnetic origin, which is obtained from FEM. The high value of the torque causes expectation that the actuator is as strong as it is expected. As the experimental results are showing considerably lower values it has been constantly speculations on validity of calculated results and the actual air-gap between rotor and stator. This has resulted a new calculation campaign where the forces and fluxes are calculated as a function of current a distance between rotor and stator (Figure 4.19, Figure 4.20).

Table 4.7 Mechanic outcome of the actuator at different excitation options

Location A, magnetization A	Location B, magnetization A	Location B, magnetization B
 <p>x-component: 111.1 N y-component: 29.8 N force angle: 15 deg force modulus: 115 N EM Torque about (0,0): 0.000 Nm Resulting torque 1.70 Nm</p>	 <p>x-component: 806.0 N y-component: 145.4 N force angle: 10.2 deg force modulus: 819 N EM Torque about (0,0): 0.069 Nm Resulting torque 8.3 Nm</p>	 <p>x-component: 588.3 N y-component: 143.4 N force angle: 13.4 deg force modulus: 606 N EM Torque about (0,0): 0.067 Nm Resulting torque 8.2 Nm</p>
 <p>x-component: 126.6 N y-component: 73.0 N force angle: 30 deg force modulus: 146 N EM Torque about (0,0): 0.000 Nm Resulting torque 4.2 Nm</p>	 <p>x-component: 1037.8 N y-component: 279.9 N force angle: 15.1 deg force modulus: 1075 N EM Torque about (0,0): 0.126 Nm Resulting torque 15.9 Nm</p>	 <p>x-component: 719.177 N y-component: 299.6 N force angle: 22.6 deg force modulus: 779 N EM Torque about (0,0): 0.135 Nm Resulting torque 17.0 Nm</p>
 <p>x-component: 112.9 N y-component: 112.8 N force angle: 45 deg force modulus: 159 N EM Torque about (0,0): 0.000 Nm Resulting torque 6.5 Nm</p>	 <p>x-component: 1101.3 N y-component: 316.2 N force angle: 16.0 deg force modulus: 1146 N EM Torque about (0,0): 0.145 Nm Resulting torque 18.0 Nm</p>	 <p>x-component: 686.5 N y-component: 377.8 N force angle: 28.8 deg force modulus: 783 N EM Torque about (0,0): 0.174 Nm Resulting torque 21.5 Nm</p>

Magnetic loading i.e. flux density distribution 0-2 T, 0.1-1.9 colored.

Saturation $\mu_r = 100$ at 1.75 T at closest loaded tooth, $\mu_r = 1200$ at 1.45T, $\mu_r = 4500$ at 0.9T

Resultant magnetic force at homopolar excitation

The magnetization direction is the same for each and every coil and this unbalances magnetomotive force variation seen along periphery. This excitation gives higher resultant force but lower load angle due to magnetically forced flux paths. In this model the rotor is moved from the centered (0.5 mm between rotor and stator) position to the horizontal rightmost alignment position (0.02 mm between rotor and stator). The resultant magnetic force and angle is presented on polar coordinate system (left), the force modulus is presented as function of machine air-gap (middle) and magnetic flux linkage is presented as function of machine air-gap (right).

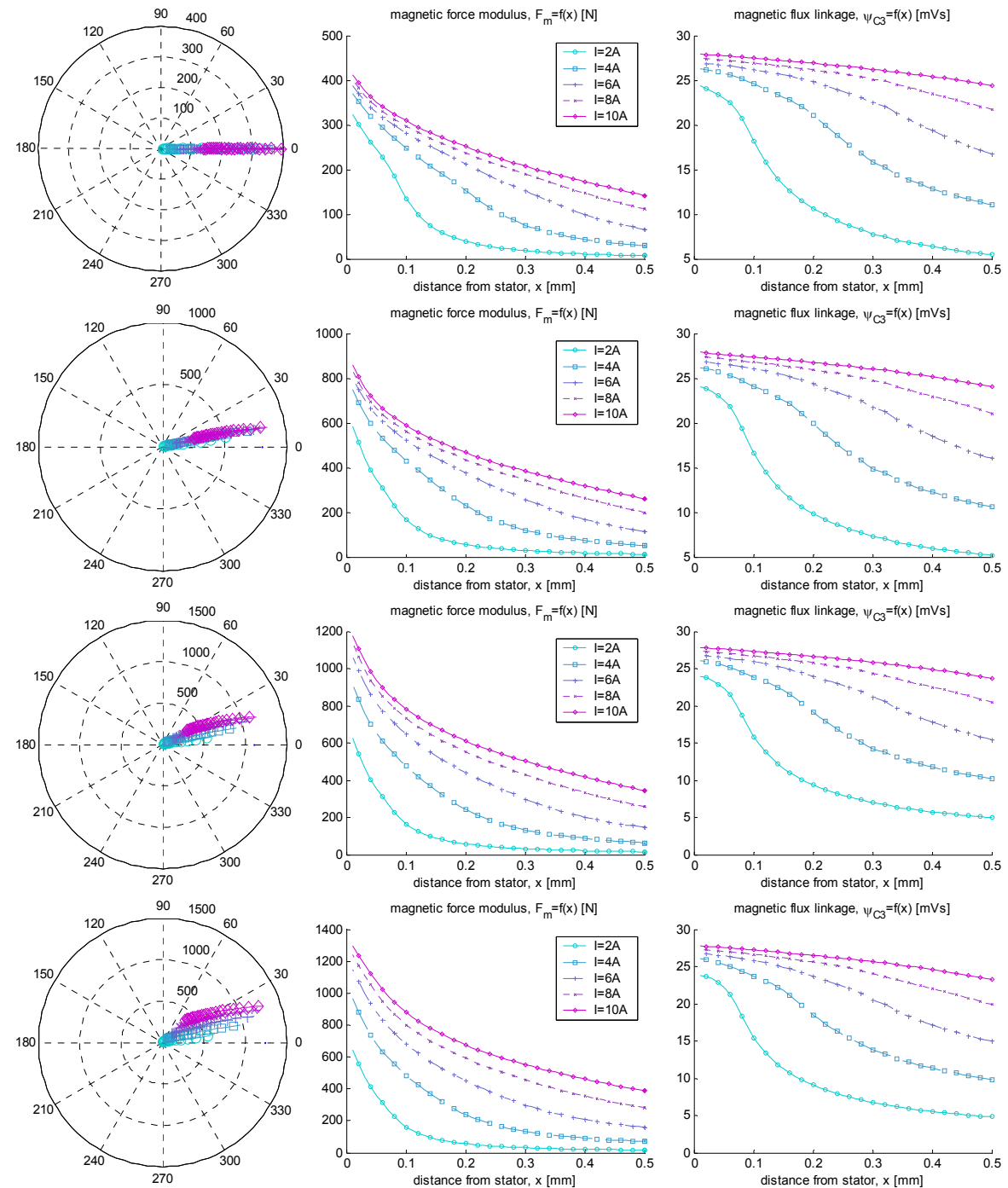


Figure 4.19 excited coils from top to bottom: A) 3, B) 2-3, C) 1-2-3, D) 12-1-2-3

Resultant magnetic force at bipolar excitation

The magnetization direction is changed every second coil and this can balance magnetomotive force variation seen along periphery. This excitation gives lower resultant force but higher load angle due to magnetically forced flux paths. In this model the rotor is moved from the centered (0.5 mm between rotor and stator) position to the horizontal rightmost alignment position (0.02 mm between rotor and stator). The resultant magnetic force and angle is presented on polar coordinate system (left), the force modulus is presented as function of machine air-gap (middle) and magnetic flux linkage is presented as function of machine air-gap (right).

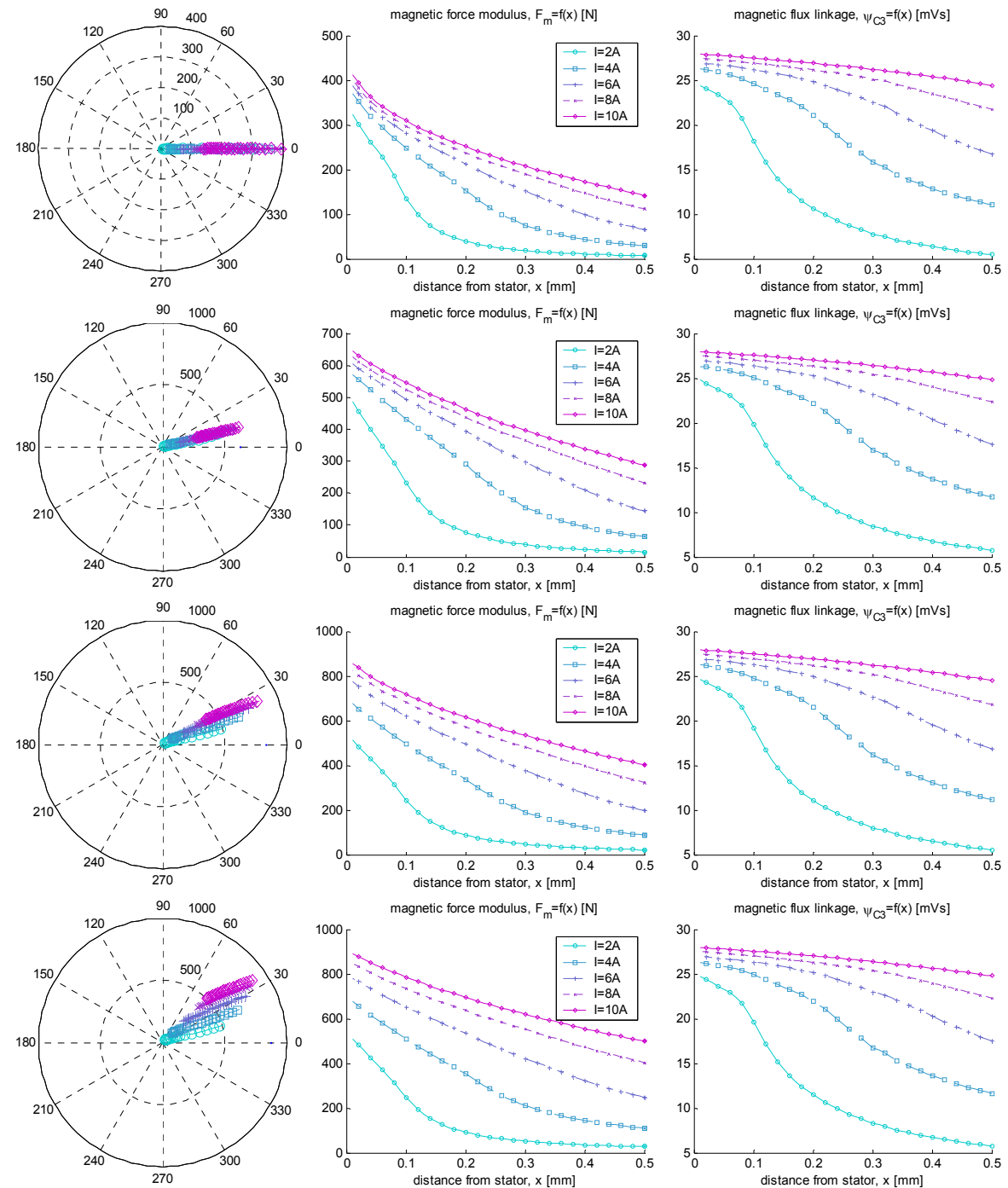


Figure 4.20 coils from top to bottom: A) 3, B) 2-3, C) 1-2-3, D) 12-1-2-3

Estimated torque

The output torque of the magnetic cycloid is estimated by using equation 4.3 and assuming that the anchor point (A) in the cycloid gear is always present independent of the air-gap in the electrical machine.

The torque is calculated according to the magnitude and the direction of the resultant magnetic force at 6 Amps excitation. Two different excitations: homopolar and bipolar are compared (Figure 4.21) with a different number of coils excited where the magnetisation direction of the coil 3 is directed to the anchor point A.

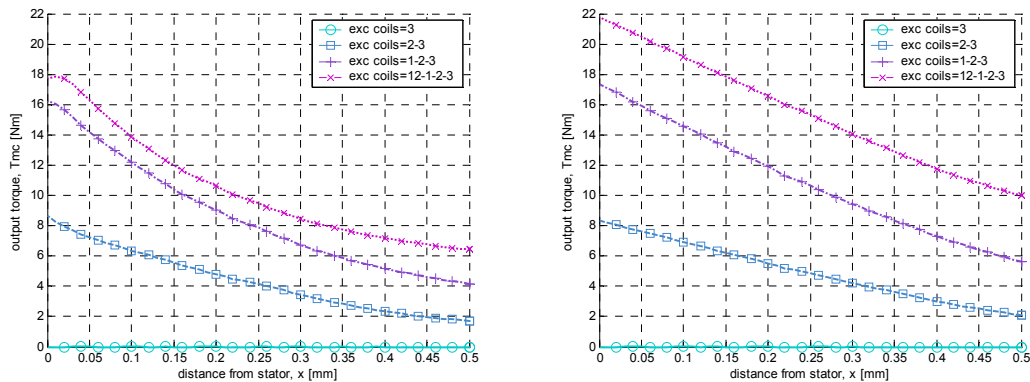


Figure 4.21 estimated torque at 6A for homopolar excitation (left) and bipolar excitation (right)

It is assumed that the peak torque is nearly the same for the minimum machine air-gap (Figure 4.21). On contrary the torque is less linear for the homopolar excitation. The calculation outcome indicates that the machine air-gap is around 0.2-0.3 mm compared to measurements with nearly 6 A providing around 3Nm external load torque of the first prototyped electromagnetic friction cycloid.

Prototyped friction cycloid configurations

Since October 2014 three different cycloid drives (Table 4.8), which are built by BEVI AB, are studied. These drives are based to the same electromagnetic configuration: 24-slot 12-coil stator Do/Di-H 120/60-75 and laminated rotor Do/Di-H 59/30-75. The difference between the drives is the cycloid gear arrangement and transmission from the eccentric disc to the output shaft.

The course of mechanical transmission development from the first cycloid transmission is to increase the inner-ring diameter of the friction cycloid disk in order to exclude the possible mechanical contact between rotor and stator and concentrate it into the transmission rings. The improvement from the 2nd prototype to the 3rd transmission is the increased friction surface and from the 3rd to the 4th transmission prototype is the doubled friction surfaces and reduced rotor diameter of 0.2 mm (Table 4.8).

Table 4.8 List over prototypes

Proto	Friction (Fr)	Cycloid disks	coupling	Remarks
1	Ø3 mm o-ring	Ø114.1+Fr / Ø116	Flange to 7 pins	Forced contact from rotor to stator
2	Ø3 mm o-ring	Ø114.7+Fr / Ø116	oldham	Higher slippage than previous
3	15 mm surface	Ø115.4 / Ø116.2	oldham	Weak performance
4	Two surfaces	Ø115.4 / Ø116.2	oldham	Expectedly improved performance

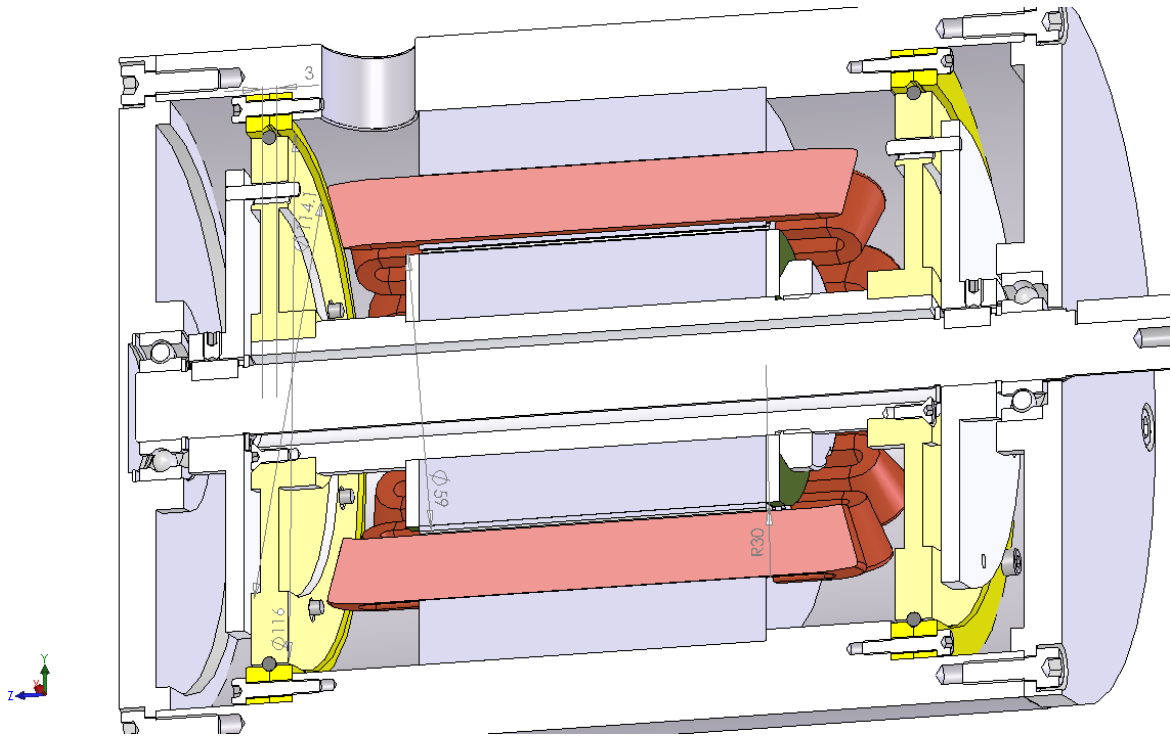


Figure 4.22 Original prototype (proto-1) with larger eccentricity and flange to pin transmission



Figure 4.23 Prototyped parts: transmission disks (left) and rotor attached to the inner transmission rings with o-ring.

The CAD drawing of the first prototype is shown in Figure 4.22 and some of the prototyped parts related to transmission in Figure 4.23.

This prototype is tested with a dc power supply with limited current at **10 A**. Experiments are made with different excitation patterns and the machine is able to produce **3 Nm** of continuous torque.

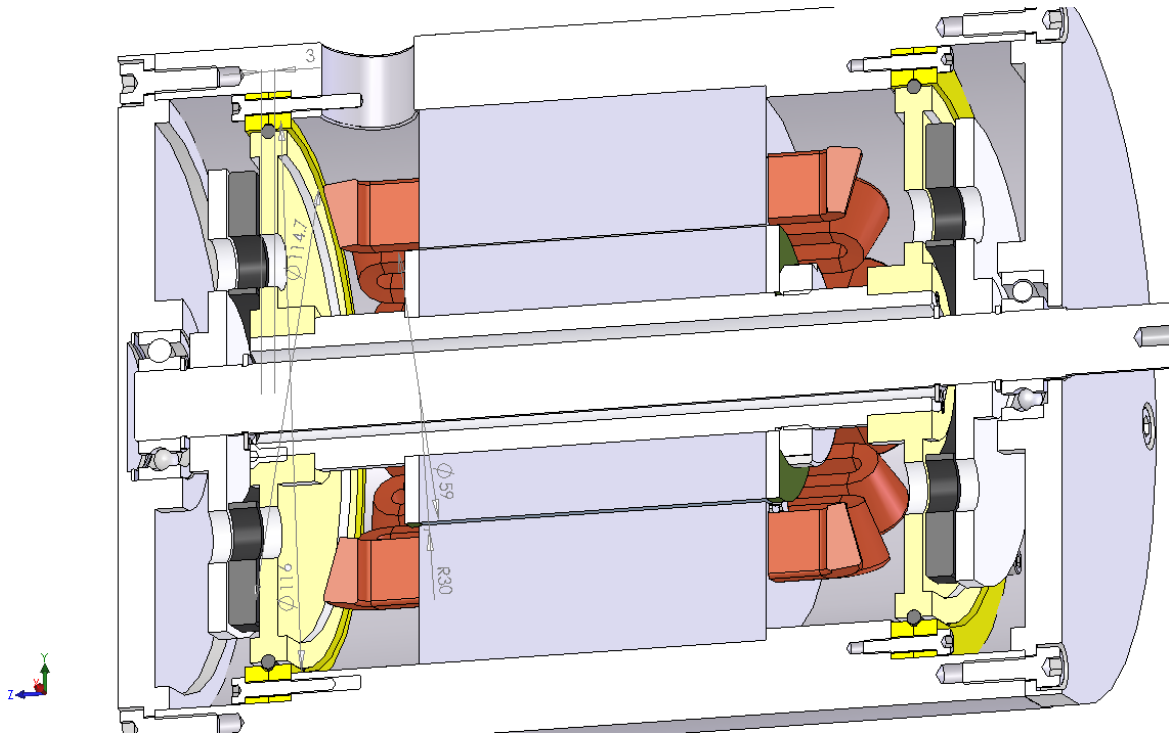


Figure 4.24 Modified prototype (proto-2) with smaller eccentricity and Oldbam coupling

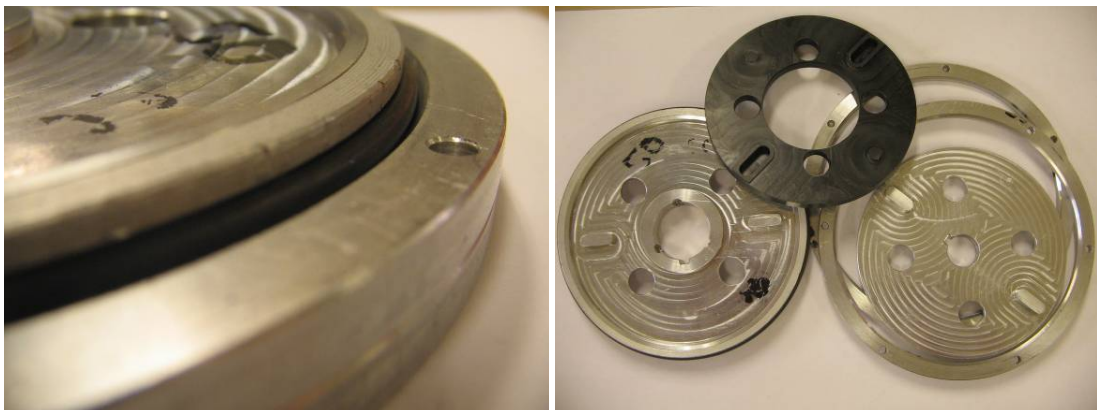


Figure 4.25 Prototyped parts for transmission: close view on the mounted transmission disks (left) and overview of the transmission part (right)

The CAD drawing of the second prototype is shown in Figure 4.24 and some of the prototyped parts related to transmission in Figure 4.25.

This prototype is tested with a dc power supply with limited current at 10 A and rectified 50Hz ac up to 40 A. Similar to previous experiments different excitation patterns are tested and the machine is able to produce 10 Nm at peak operation conditions.

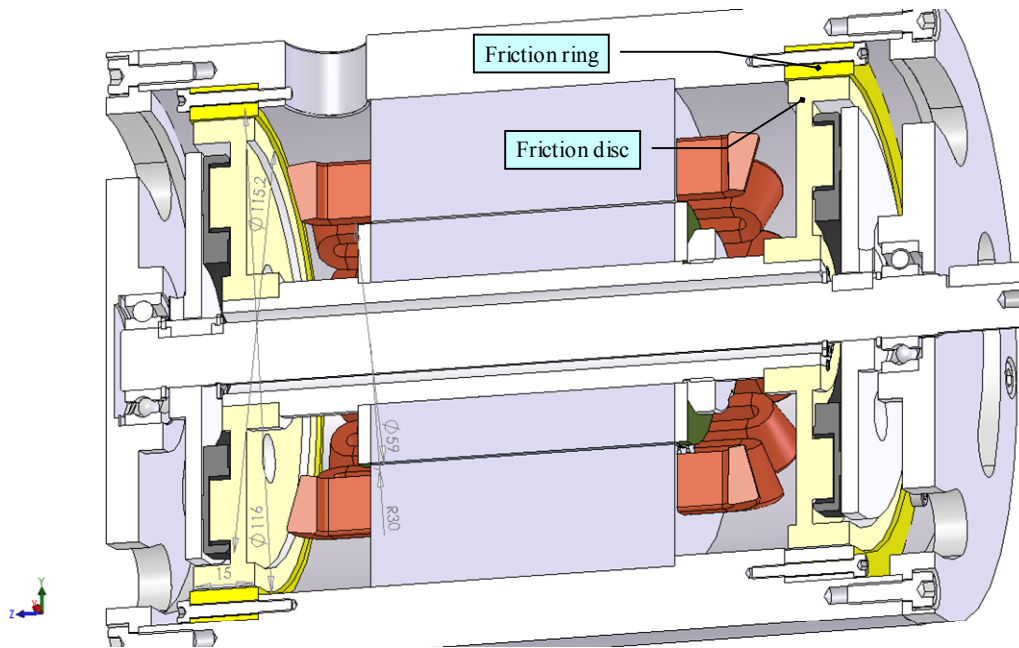


Figure 4.26 Remodified prototype (proto-3) with friction surfaces instead of o-ring

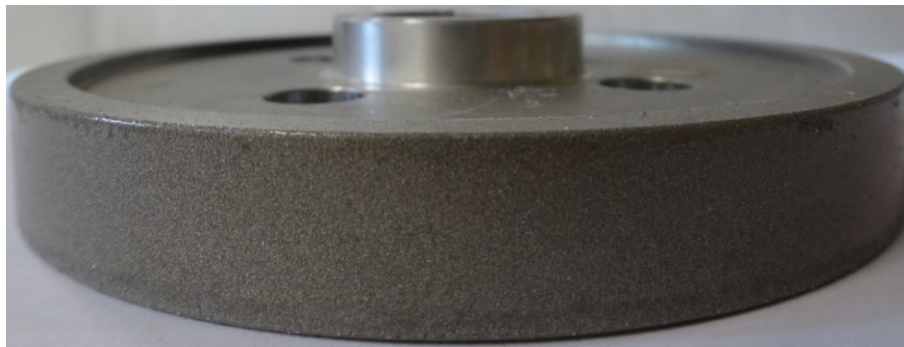


Figure 4.27 Friction disc with 125-250 μ m friction layer



Figure 4.28 Friction ring

The CAD drawing of the third prototype is shown in Figure 4.26 and some of the prototyped parts related to transmission in Figure 4.27 and Figure 4.28.

This prototype is tested with a rectified 50Hz ac up to **30 A**. Similar to previous experiments different excitation patterns but this machine has never exceeded **1 Nm** for the same conditions as previous experiment.

The transmission rings are carefully observed in order to clarify the reason why the increased friction area has resulted lower output torque. The friction disc (Figure 4.27) is inside a friction ring (Figure 4.28). These two surfaces are inspected visually and cleaned with a paper napkin. The purpose of doing that is 1) inspect whether the surfaces contain metallic dust as a sign of wearing

off or dilapidation, 2) estimate a cognitive friction of the corresponding surfaces. As an explanation it is expected that the slippery surface of the outer ring limits the ability to hold the connection point (equation 4.4) or alternatively the torque shoulder has become considerably shorter for the same electromagnetic forces. Therefore the fourth prototype is built where both inner ring as well as the outer transmission ring has a thin layer (0.1 mm) of a rubber like friction coating (Figure 4.27 and Figure 4.28).

Conclusions based on observations

- The attrition or wearing away of the friction layer of the friction disk neither the material wear from the friction ring is inconsiderable.
- There is a fine frictional drag when wiping the friction surface of the friction disk
- There is a considerably lower frictional drag from the inner surface of the friction ring, considered as a slippery surface.

If the first prototype could bring the rotor into the mechanical contact to the stator then the air-gap is measured for the other prototypes and it has been found that the gap is always 0.15-0.2 mm at the loaded condition.

Frictional EMCD - measurements

The main goal for the experimental evaluation is to quantify the torque capability of the electromagnetic cycloid drive (EMDC). Therefore the detailed analysis of control sequence, optimal current control as well as force and torque waveforms have a minor interest.



Figure 4.29 Experimental setup on the left figure: from the left 1) PC provides switching sequence to 2) relay card that is 3) supplied from DC voltage source and excites 4) the coils of the prototype motor which is 5) loaded with external weight on the load wheel. Rectified ac supply is used on the right figure.

The measurement setup is photographed at running condition where the supply of 0.1 sec sample rate (50 rpm as the magnetization input) turns the load wheel 0.2-0.25 rpm. Some observations of the horizontal cycloid machine are made:

- Gravity plays important role for uncompensated current supply where the magnitude of the current is kept constant. This means that the machine loses grip due to heavy load or weak supply when rolling upwards the rotor
- Slip becomes more dominant at heavy load or a weak supply that is seen as a reduction of the rotation speed at the same supply frequency.

Actuator initialization

A number of measurements are made on the cycloid motor for the purpose of initializing the test object at a ground based rotor. Coil resistance and inductance are the quantities that are directly measured by using a multimeter AMPROBE-LCR55A. The stall force/torque is sensed and not quantified. O-ring compression is measured as a function of vertical load in BEVI.

The resistance of coils are 0.23 ± 0.01 Ohm, which compares quite well of the theoretical value of resistance (0.23 Ohm) $R = 1.75e-8 * N^2 * lw / Aw$, where $N = 45$ turns, $Aw = 2 * N * \pi * 0.71e-3^2 / 4$ is total copper area, and $lw = 2 * (97e-3 + \pi * 6e-3)$ average turn length.

The inductance depends on the location of the teeth where the coil is placed and the actual air-gap between this teeth and the rotor. Due to gravity the inductance is different (Figure 4.30) and it has some variation when rotating the rotor for the same position of the coil. Theoretically the inductance is $L = \mu_0 \cdot \mu_{eff} \cdot N^2 \cdot A_c / l_c$, where $A_c = 4e-3 \cdot 75e-3 \cdot 0.95$ is magnetic cross-section area of teeth, $l_{fe} = 2 \cdot 15e-3 + \pi / 12 \cdot (75e-3 + 60e-3)$ is magnetizing path in the core, l_{gap} is magnetizing path in the air-gaps and μ_{eff} is the effective permeability of core+air-gap.

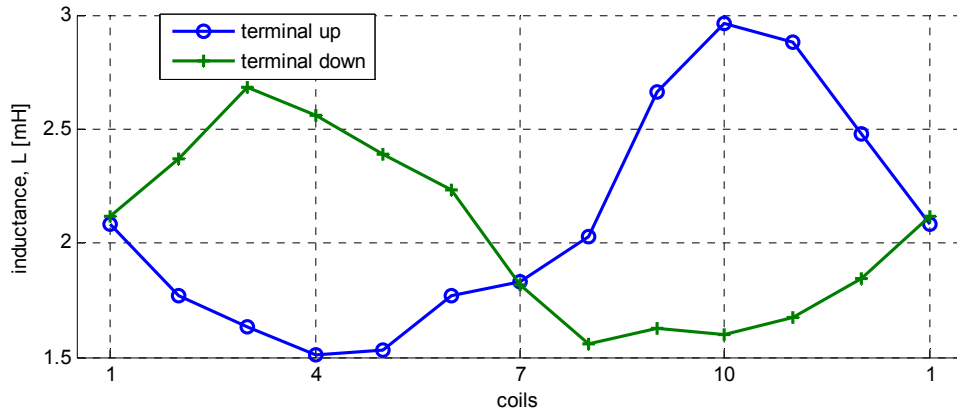


Figure 4.30 measured inductance of the coils when the machine is placed so that terminals are vertically upwards and oriented downwards.

Inductance measurement for determining the air-gap distance

In this measurement the stator coil with smallest and largest inductance is detected. It is expected that the coil with largest inductance lies beneath the rotor having the narrowest air-gap and the coil with the smallest inductance has the largest air-gap. It is detected that for this occasion the coil 3-4 had the largest inductance and the coil in the opposite side 13-14 had the smallest inductance. The next step in this measurements is to apply and increase the current of this coil that had the largest inductance (= smallest air-gap), and to measure the inductance of these two adjacent coils. The measurement results are presented in Table 4.9.

Table 4.9 measured inductance as a function of voltage and current

Supply voltage, V	Supply current, A	Single coil excited		Two coils excited	
		Bottom coil inductance, mH	Top coil inductance, mH	Bottom coil inductance, mH	Top coil inductance, mH
0.0	0	3.13	1.5	3.12	
0.8	0.6	3.12	1.51	3.14	
1.1	1.4	3.11	1.51		
1.2	1.7	3.09	1.52	2.90	
1.4	2.3	3.01	1.52		
1.5	2.6	2.98	1.54		
1.6	2.8	1.74	2.34	1.82	
1.8	3.3	1.62	2.73		
2.0	4.0	1.59	2.78	1.63	
2.1	4.2	1.58	2.82		
2.2	4.5	1.57	2.83	1.61	
2.5	5.6	1.56	3.03	1.61	
2.8	6.4	1.56	3.03		
3.0	6.7	1.56	3.03		
3.1	7.1	1.55	3.03		
4.2	10	1.55	3.13		

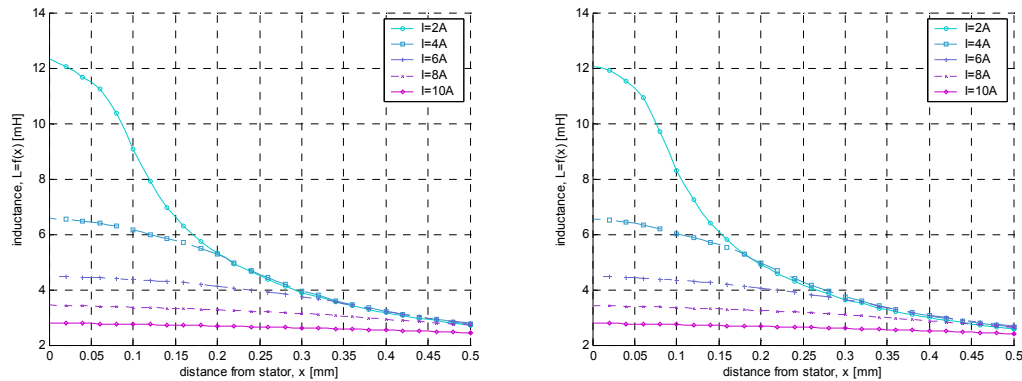


Figure 4.31 Inductance of the coil for the alignment pole as a function of current and rotor position from the pole. Single coil excitation is considered in the left and two-coil excitation is shown in the right.

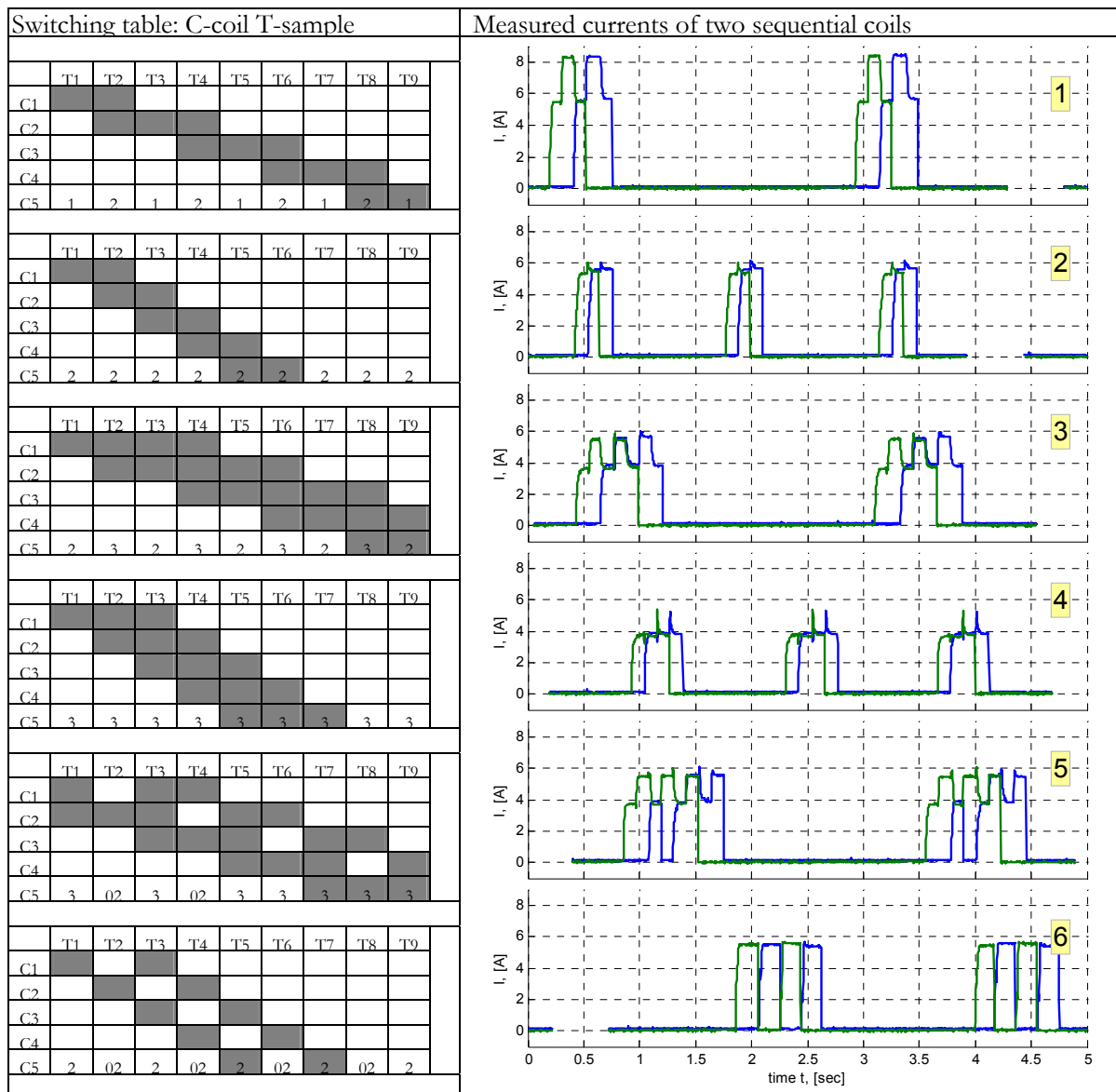
When investigating the calculated inductance curves (Figure 4.31) then it is noticed that the calculated inductance at high current and small gap is considerably higher than the measured one. Due to that reason it is hard to speculate on the resultant machine air-gap of the loaded system.

Torque capability

The process of studying the test object is listed below. The ultimate goal is to determine torque capability as a function of supply.

1. Supply voltage (and current) is progressively increased so that the outcome of the excited the machine coils results not only the rotor to be lifted and able to carry its own weight but also rotate and lift the external loads of 1, 2, 3 up to 8-10 kg. The external test wheel has a groove at 20 cm in diameter.
2. Slip is studied as a function of current and load before the rotor starts to loose a grip. It takes around 90 sec to turn 90 degrees at 20 0.1 sec samples per electric revolution when using the excitation pattern 1 for the prototypes. Later a number of measurements have been increased as the time readings were recorded every 10 degrees of motion.
3. The excitation pattern1 is compared to excitation pattern 2. Less current is needed to lift the same amount of load.
4. Other excitation patterns (1, 3-6) are not able to lift the weight at the same dc-link supply conditions.
5. The switching sequence where a larger number of coils than 3 are involved becomes rather rapid and weak where the machine is not able to hold the rotor – there is not enough thrust to accelerate the mass in desired direction.

Table 4.10 Excitation patterns and magnitude of reference current (pattern 1 and 2) for providing 3 Nm (for proto-1)



Output speed as a function of current and load torque is measured for different prototypes. As it is now there are obvious limitations

1. Most of the proto-1 measurements are limited by 10 A dc
 - a. Test sample: 2.5V, 3A, 2kg, 90 deg, 90 sec – 2 switches continuously lighted,
 - b. Test sample: 3.0V, 5A, 3kg, 90 deg, 135 sec– 2 switches continuously lighted
2. Proto-2 is measured both with dc and rectified ac source and is the most measured prototype
 - a. Test runs: 10-30A, 1-8kg, a number of measurements over 10 deg angle – 2, 3 and 4 switches continuously lighted (Figure 4.32)
 - b. Peak operation 40A is able to provide 10Nm by lifting 10kg load – 3 and 4 switches continuously lighted

3. Proto-3 measurements are carried out at very limited region: 12-30 A rectified ac with 1 Nm load only. There is no chance to provide any positive rotation at any higher load

The electric excitation cycle has 12 pulses 0.1 sec per pulse which is 50 rpm electric speed. The mechanical outcome is at least 250 times lower. The high speed ratio is not directly outcome of the “high” gear ratio rather than loss of speed due to slippage. Eqvi torque lines shown in Figure 4.32.

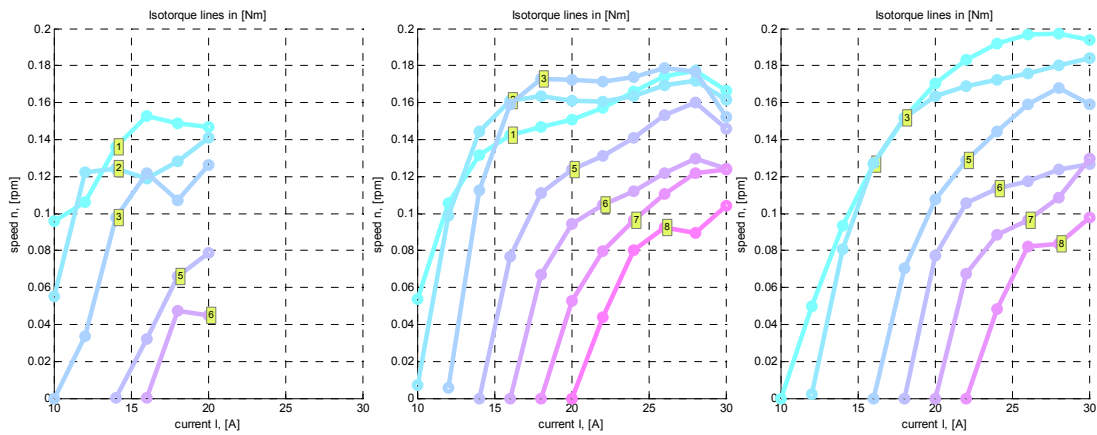


Figure 4.32 Measured torque-speed characteristics of proto-2 with different excitation sequences: output speed as a function of: left: 2-coils energised, middle 3-coils and right: 4-coils energised.

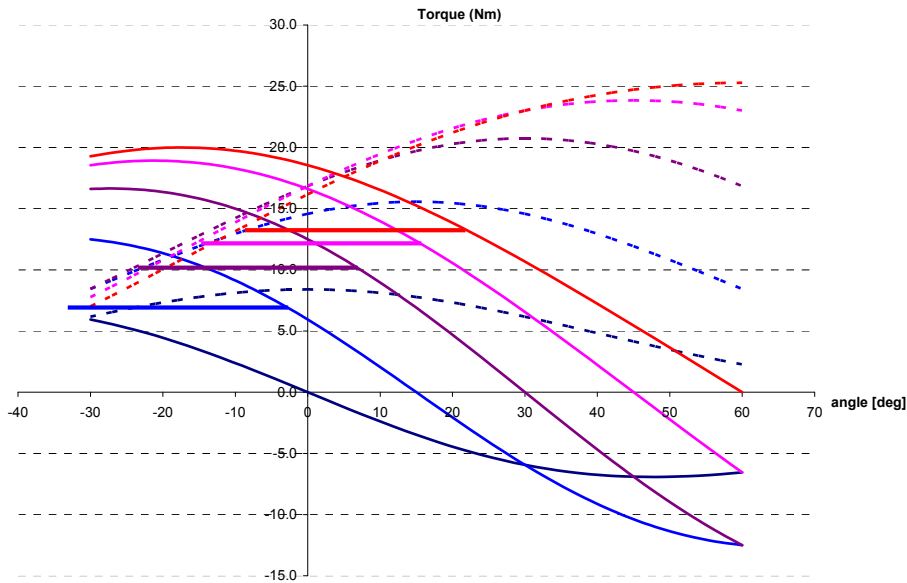


Figure 4.33 Torque capability as an outcome of the driving torque (solid lines) and the supported transmission torque (dashed lines) results the output torque (solid horizontal lines) over the 30 degrees angle where coils are energized. Dark blue shows the contribution of the coil straight under the connection point (normal forces only). Red line shows the expected torque curves when 5 sequent coils are energized.

The outcome of the driving torque from magnetic forces point of view and the holding torque from mechanical transmission support or hold point of view is analyzed by using equations 4.3 and 4.4. As the magnetic forces are applied to roll and revolve the rotor the force action point is changed relative to the friction and the applied normal forces to this point. This support changes the ability to transmit the driving torque to the output shaft. In this calculation the radius of the inner friction ring is 57 mm and the friction factor is taken 0.6.

4.3 Control and selection of power electronic controller

There have been a number of discussions on developing a driver board from minimum of 1 switch, by following examples for switched reluctance drives, up to 4 switches (H-bridge) per single coil in the machine. All these drivers could have their own current control or a switching pattern at limited voltage. The control unit could be NI Rio that gives powerful sources to make advanced control.

Alternatively, more autonomous controllers and existing standard driver modules have been studied.

Control realization on dsPIC33EP512GM710 provides not only 6 PWM channels but also other features with low price, which might perfectly suit for the cycloid drive. More information in <http://edn.com/electronics-products/other/4425582/Digital-signal-controllers-support-dual-motor-control-applications>. The advantage is taken of a development board that limitations are that this board suits for conventional BLDC and PMSM 48V/15A machines. Alternatively IRAMS06UP60B (or a similar unit with another rating) is selected for driving the machine or controller circuit with one switch per phase that is analyzed for the specific drive application.

Finally a relay card with 16 relays have been invested that reduces the implementation time to minimum and allowed to test 7-8 switching patterns, that usually included 12 combinations per magnetization revolution with the smallest step of 0.1 sec.

5 Conclusions

The goal of this project is a development of an actuator for Automatic Transmission Shifted by Wire (ATSbW). Direct electromagnetic actuators based on magnetic interaction and on the material elongation are studied and realized that the actuators are not the best option for ATsbW application. The study and integration depth on unconventional actuators has been taking the unusual approach of taking advantage of normal magnetic forces. This has resulted to a direct magnetic strain wave gearing in a harmonic drive and direct magnetic relocation of the cycloid disk in a cycloid drive. None of the drives has been finalized as a working prototype despite advanced modeling. Definitely the valuable design experience on electrical and mechanical engineering should be used to define a set of speed reducers for rapid prototyping that can be used for learning mechatronics and getting inspiration for industrial challenges in robotics, drives for vehicular appliances and so on.

During a course of project there is a continuous development behind the electromagnetic frictional cycloid to learn the challenges of direct magneto mechanical transmission (Figure 5.1 and Table 5.1). The course of achievements has not led to perfect solution for ATsbW application rather than created valuable experience on design and integration of unconventional electromagnetic actuators.

Table 5.1 Prototype transmission modifications and outcomes

Proto	Friction (Fr)	Cycloid disks	coupling	Torque per coil ampere
1	Ø3 mm o-ring	Ø114.1+Fr / Ø116	Flange to 7 pins	3 Nm / 5 A (2 coils per step)
2	Ø3 mm o-ring	Ø114.7+Fr / Ø116	oldham	3 Nm / 7 A (2 coils per step)
3	15 mm surface	Ø115.4 / Ø116.2	oldham	1 Nm / 8 A (2 coils per step)
4	Two surfaces	Ø115.4 / Ø116.2	oldham	Poor friction for transmission

One outcome of this project is the indication that the direct magnetic actuation either on gears or output axle is not shortest way of providing unconventional and smart technical solutions. At the same time the investigation, research and development of unconventional electromagnetic actuators gives a new sight not only on the history of electrical machines but also the advancement on electromechanical actuators and magnetic materials used in these devices. This in turn influences directly modeling and design, and in continuation application oriented control, integration and implementation. Therefore, the learning outcome results some intriguing models for visualizing and developing ideas and concerns related to some types of unconventional electromechanical transmission integrated actuators.



Figure 5.1 Prototype

References

- [1] Chicurel-Uziel, R., "Cycloidal Magnetic Gear Speed Reducer", *Modern Mechanical Engineering*, 2013, 3, 147-151
- [2] Claeysen, F., Lhermet, N., Le Letty, R., Bouchilloux, P., "Actuators, transducers and motors based on giant magnetostrictive materials", *J. Alloys and Compounds*, 258 (1997) 61-73
- [3] Dong, H., Ting, K.-L., Wang, D., "Kinematic Fundamentals of Planar Harmonic drives" *J. Mechanical Design*, ASME, Vol 133, Jan. 2011, 011007 1-8
- [4] Dong, H., Zhu, Z., Zhou, Z.C. "Dynamic simulation of harmonic gear drives considering tooth profiles parameters optimization", *J. Computers*, Vol 7, no 6, June 2012, pp. 1429-1436
- [5] Hollerbach, J. M. et al., "A comparative analysis of actuator technologies for robotics," in *Robotics Review 2*, ed Cambridge, MA: MIT Press, 1991, pp. 299-342.
- [6] Ladufjäll, E. "Evaluation of a magnetic harmonic traction drive", MSc thesis, KTH, 2008
- [7] Li, X. et al., "A new cycloid drive with high-load capacity and high efficiency," *Journal of Mechanical Design*, vol. 126, pp. 683-686, Jul 2004.
- [8] Malhotra, S.K, Parameswaran, M.A "Analysis of a cycloid speed reducer", *Mechanism and Machine Theory*, Vol 18, Issue 6, 1983, Pages 491-499
- [9] Radzevich, S.P., Dudley, D.W. "Handbook for practical gear design", CRC press, New York 2012
- [10] Sensinger, J. W. "Unified approach to cycloid drive profile, stress, and efficiency optimization," *ASME Journal of Mechanical Design*, vol. 132, pp. 1-5, 2010.
- [11] Sensinger, J.W., Lipsey J.H. "Cycloid vs. harmonic drives for use in high ratio, single stage robotic transmission". *IEEE Int Conf Robotics and Automation*, May 14-16, 2012, pp. 4130.
- [12] Song, Yuan; Qizheng Liao; Shimin Wei; Lei Guo "Research on pure rolling cycloid-like reducers used in industrial robot", *Information and Automation (ICIA)*, 2014 IEEE International Conference on, On page(s): 305 - 310
- [13] Taghirad, H. D. and Belanger, P. R., "Modeling and parameter identification of harmonic drive systems," *Journal of Dynamic Systems Measurement and Control-Transactions of the ASME*, vol. 120, pp. 439-444, DEC 1998.
- [14] Tellinen, J., Suorsa, I., Jääskeläinen, A. Aalto, I. And Ullako, K., "Basic properties of magnetic shape memory actuators", *Int Conf Actuator*, Bremen, Germany, 10-12 June 2002
- [15] Tuttle, T. D. "Understanding and modeling the behavior of a harmonic drive gear transmission," M.S., *Mechanical Engineering*, Massachusetts Institute of Technology, 1992.
- [16] Willis, R.J., "Lightest-weight gears" *Product Engineering*, Jan 21, 1963, pp 64-75
- [17] Yang, D. C. H. and Blanche, J. G. "Design and application guidelines for cycloid drives with machining tolerances," *Mechanism and Machine Theory*, vol. 25, pp. 487-501, 1990.